Cellular stress in vitro and longevity in vivo

Dekker, P.

Chapter 6

Microarray-based identification of age-dependent differences in gene expression of human dermal fibroblasts

Pim Dekker, David Gunn, Tony McBryan, Roeland W. Dirks, Diana van Heemst, Fei-Ling Lim, Aart G. Jochemsen, Matty Verlaan-de Vries, Julia Nagel, Peter D. Adams, Hans J. Tanke, Rudi G.J. Westendorp, Andrea B. Maier

Submitted for publication

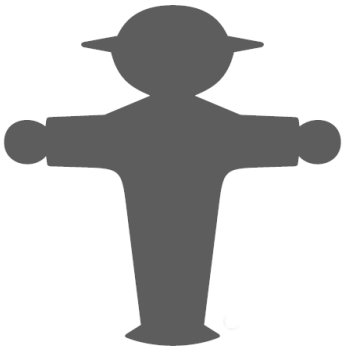

Summary

Senescence is thought to play an important role in the progressive age-related decline in tissue integrity and concomitant diseases, but not much is known about the complex interplay between upstream regulators and downstream effectors. We profiled whole genome gene expression of non-stressed and rotenone-stressed human fibroblast strains from young and oldest old subjects, and measured Senescence Associated-β-gal (SA-β-gal) activity. Microarray results identified gene sets involved in carbohydrate metabolism, Wnt/β-catenin signaling, the cell cycle, glutamate signaling, RNA-processing and mitochondrial function as being differentially regulated with chronological age. The most significantly differentially regulated mRNA corresponded to the p16 gene. p16 was then investigated using qPCR, Western blotting and immunocytochemistry (ICC). In conclusion, we have identified cellular pathways that are differentially expressed between fibroblast strains from young and old subjects.

Introduction

In addition to apoptosis, senescence is thought to contribute to the progressive age-related decline in tissue integrity and the concomitant diseases (1). It was found that various types of stressors (e.g. cytokines, oxidative agents) could induce premature senescence, implying a significant role for environmental factors in accelerating the aging process. In the past, studying senescence *in vivo* was thwarted by the lack of markers that indubitably identify senescent cells. Meanwhile studies into the signal transduction pathways of senescence have led to identification of many proteins that have overlapping roles in senescence, apoptosis and DNA-damage sensing (2).

Despite the fact that senescence, apoptosis and DNA-damage repair have been shown to play pivotal roles in the aging process, not much is known about the complex interplay between upstream and downstream pathways that operate intracellularly and between tissues on the systemic level. Gene expression array technologies may help to find a specific profile of differential gene expression as a marker of senescence. Comparisons of gene expression profiles have been made between various tissues of chronologically young and old mammalian model organisms (3-13) and humans (14-24). These studies show that different tissues in various species show similar changes in expression of genes involved in DNA-damage repair, cell cycle progression, senescence, apoptosis, stress response, immune response and metabolism. However, there are also many species-dependent and tissue-dependent differences that these studies did not address, and it is also not clear which changes are the results of the aging process and which drive the aging process. We have already reported that human skin fibroblast strains derived from chronologically young subjects, when compared with fibroblast strains from oldest old subjects (90 years of age), are less prone to go into senescence and more prone to go into apoptosis, both under non-stressed and stressed conditions (25). Also, fibroblast strains from middle aged offspring of nonagenarian siblings exhibited less senescence and more apoptosis when compared with fibroblasts from the partners of the offspring, representing the general population. Thus, fibroblasts from the offspring demonstrated younger cellular characteristics than fibroblasts from age-matched controls.

Here, we aimed to identify the cellular pathways that drive the differences with chronological age in cell senescence and apoptosis. We performed whole genome gene expression profiling of non-stressed and rotenone-stressed human fibroblast strains from young and old subjects. We expected the rotenone treatment to exacerbate differences in gene mRNA levels with age and, in particular, affect genes involved in senescence, apoptosis, DNA-damage repair, cell cycle progression, stress responses and metabolism. We validated the most significant mRNA change by qPCR and then performed a replication experiment in independent strains to investigate whether mRNA changes were reflected by protein level changes.

Material and methods

Study design

The Leiden 85-plus Study (26) is a prospective population-based study in which all inhabitants aged 85 years or older of the city of Leiden, the Netherlands, were invited to take part. Between September 1997 and September 1999, 599 out of 705 eligible subjects (85%) were enrolled. All participants were followed for mortality and 275 subjects survived to the age of 90 years. During the period December 2003 up to May 2004, a biobank was established from fibroblasts cultivated from skin biopsies from 68 of the 275 surviving 90-year-old participants (27). These participants were in good physical and mental condition and were able to come to the research institute, where the same qualified physician carried out the procedures. During the period August to November 2006, we also established a biobank of fibroblast strains established from biopsies taken from 27 young subjects (23-29 years old).

Fibroblast cultures and experimental setup

Three-mm biopsies were taken from the sun unexposed medial side of the upper arm. Fibroblasts were grown in D-MEM:F-12 (1:1) medium supplemented with 10% fetal calf serum (FCS, Gibco, batch no. 40G4932F), 1 mM MEM sodium pyruvate, 10 mM HEPES, 2

mM glutamax I, and antibiotics (100 Units/mL penicillin, 100 µg/mL streptomycin, and 0.25–2.5 µg/mL amphotericin B), all obtained from Gibco, Breda, the Netherlands. This medium will be referred to as standard medium. Fibroblasts were incubated at 37^{o}C with 5% CO_2 and 100% humidity. All cultures that are used in the present study were grown under predefined, highly standardized conditions as published earlier (27) and frozen at low passage. Trypsin (Sigma, St Louis, MO, USA) was used to split fibroblasts using a 1:4 ratio each time they reached 80-100% confluence.

Passage 11 fibroblasts were thawed from frozen stocks on day zero. On day four, seven and 11 fibroblasts were further passaged in order to multiply fibroblasts. On day 18 the experiments were started. For the microarray experiments, fibroblast strains were seeded at 5200 and 7500 cells/cm^2 for non-stressed and rotenone-stressed cultures respectively. For the replication experiments, fibroblast strains were seeded at 2300 and 3900 cells/cm^2 for non-stressed and rotenone-stressed cultures respectively. Strains were seeded in batches of eight strains per condition.

To chronically stress fibroblast strains, medium was supplemented with 0.6 µM rotenone (Sigma, St Louis, MO, USA), known to induce an increase in the intracellular production of reactive oxygen species (ROS) at the mitochondrial level (28). After three days fibroblast strains were assessed for SA-β-gal, ROS, microarray experiments, p16 on the mRNA level and the protein level as described below. In order to check early response genes samples were also taken at three hours for the microarray experiments.

Flow cytometric measurement of SA-β-galactosidase activity

Fibroblasts were prepared as described earlier (29). In short, to change the lysosomal pH to pH 6, fibroblasts were incubated with medium containing 100 nM bafilomycin A1 (VWR, Amsterdam, the Netherlands) for 1 hour. Fibroblasts were then incubated with 33 µM of the β-galactosidase substrate C_{12}FDG (Invitrogen, Breda, The Netherlands), in the presence of 100 nM bafilomycin. After trypsinisation, fibroblasts were washed once and resuspended in 200 µl ice cold PBS. Fibroblasts were measured in the FITC-channel and analysis was performed on the Median Fluorescence Intensity (MdFI) values.

Flow cytometric measurement of ROS

Fibroblasts were incubated in medium supplemented with 30 µM dihydrorhodamine 123 (Invitrogen, Breda, The Netherlands). They were then trypsinized, washed in ice-cold PBS, pelleted and resupended in 200 µl ice-cold PBS. Fibroblasts were kept on ice before measurement of MDI in the FITC-channel.

Microarray Analysis

All products were purchased from Agilent Technologies UK Ltd (Wokingham, Berkshire, UK) and used according to manufacturer's protocol unless stated otherwise. All samples (n=12) were isolated and run on microarrays separately. Total mRNA was isolated using the RNeasy Mini Kit (Qiagen Ltd, Crawley, UK) and 300ng was mixed with an appropriate amount of One-Color RNA Spike-In RNA and converted into labelled cRNA (One-Color Low RNA Input Linear Amplification Kit PLUS). Labelled cRNA was purified using an RNeasy Mini Kit (Qiagen Ltd, Crawley, UK) and 2µg was hybridised to Agilent human whole genome Oligo Arrays (G4112F; 41094 probes) using reagents supplied in the Agilent Hybridisation Kit (One-Color Microarray-Based Gene Expression Analysis Protocol). Microarray slides were hybridised for 17 h at 65 ºC and subsequently washed in acetonitrile for 1 min followed by 30s in Agilent Stabilisation and Drying Solution. Scanning of the slides was performed with the Agilent G2565BA Microarray Scanner System. The Agilent G2567AA Feature Extraction Software (v.9.1) was used to extract data and check the quality. To comply with MIAME requirements the data discussed in this publication have been deposited in NCBI's Gene Expression Omnibus (GEO) (30;31) and are accessible through GEO Series accession number GSE28300 (http://www.ncbi.nlm.nih.gov/geo/query/acc.cgi?acc=GSE28300).

Validation/replication of p16 by qPCR

cDNA syntheses of total RNA extracted from non-stressed fibroblast strains or rotenone-stressed fibroblast strains was carried out using 0.5µg total RNA per reaction. Synthesis of cDNA was via AMV first strand synthesis kit (Roche Applied Science, Hertfordshire, UK) according to the manufacturer's instructions. All PCR mixes were prepared in triplicate, comprising 0.1µl of freshly prepared cDNA, 1 x SYBR Green PCR master mix (Bio-Rad Laboratories Ltd, Hemel Hempstead, UK) and 1 x QuantiTect PCR primers (Qiagen Ltd,

Crawley, UK) specific for the genes CDKN2A/p16 (QT00089964) or to PPIA/cyclophilin A (QT00062311). Semi-quantitative PCR was performed on a Bio-Rad iCycler. Transcript levels were normalized to PPIA and data analysis was performed using the comparative cycle threshold method (ΔΔCT).

p16 immunoblotting

Fibroblasts were lysed in RIPA buffer (20mM Triethanolamine-HCL, ph 7.8, 140 mM NaCl, 0.1% Natrium deoxycholaat, 0.1% Natrium dodecylsulfaat (SDS) and 0.1% Triton X-100) with protease inhibitors (SIGMA*FAST* ™ Protease Inhibitor Cocktail Tablets, EDTA-free) used according to the manufacturer's protocol. Proteinlysates of the fibroblasts were stored at -80℃. Protein content was determined by Pierce BCA Protein Assay Kit (Thermo Scientific, Breda, the Netherlands). Proteins were fractionated by 10% and 15% SDS-polyacrylamide gel electrophoresis. For every strain the loaded amounts of protein were the same for the unstressed and for the rotenone-stressed condition. Samples of three subjects were not used for immunoblots because of very low protein content. Proteins were blotted onto a PVDF membrane (Immobilon-P, Millipore, Billerica, USA). Membranes were blocked in Tris-Buffered Saline Tween-20 (TBST) containing 10% non-fat dry milk. Primary antibodies were prepared in TBST solution with 10% dry milk. Membranes were incubated overnight at 4℃ with the following primary antibodies: α-p16 JC8 (Santa Cruz Biotechnology, 1:500) and α-Hausp Pab (Bethyl laboratories, Montgomery 1:1000). After incubation, membranes were washed three times with TBST and incubated with goat anti-mouse or goat anti-rabbit antibody coupled to horse-radish-peroxidase for one h at room temperature. Antibody binding was visualized using Super Signal West Dura (Thermo Scientific, Breda, the Netherlands) and exposure to X-ray film. The software package Odyssey (LI-COR Biosciences, Lincoln, USA) was used to quantify the values from the Immunoblot signals, the values of which were expressed in arbitrary units (AU). All values were normalized for loading control before they were used further for statistical analyses.

Immunocytochemical staining for p16

Fibroblasts were fixed with 4% paraformaldehyde in PBS for four minutes. After permeabilization for 20 minutes in 0.2% Triton (Sigma, St Louis, MO, USA) in PBS, samples were

blocked with blocking buffer (3% BSA in PBS) for one hour at room temperature and incubated for two hours with anti-p16 (JC8) antibody (Santa Cruz Biotechnology Inc., Santa Cruz, USA), diluted 1/100 in blocking buffer. After five washes with PBS, cells were treated with 0.3% H_2O_2 in methanol to reduce background peroxidase activity. Fibroblasts were then stained using an anti-mouse IgG Vectastain Elite ABC kit (Vector laboraties, Burlingame, CA, USA) and a DAB Peroxidase Substrate Kit (Vector laboraties, Burlingame, CA, USA), according to the manufacturer's protocols. Fibroblasts were counterstained with Hematoxylin (Vector laboraties, Burlingame, CA, USA) for five minutes and incubated with NH4OH in 70% ethanol for one minute. After washing in water, slides were mounted with Faramount Mounting Medium (DAKO, Heverlee, Belgium) and photographed with a Leica microscope (Leica Microsystems, Rijswijk, the Netherlands). Per sample 500 randomly chosen cells were assessed for p16 positivity.

Statistics

Raw data produced from microarrays were imported into R version 2.11.0 (2010-04-22) (32), an open source statistical analysis program, using custom code. Background correction was performed using the normexp+offset method and data were log-transformed (33). Differential expression of genes was determined by fitting a linear model using the lmFit function from the limma package and moderated t-statistics were computed using the ebayes function (34). The linear model included parameters for treatment, age, gender and batch effects. Bonferroni-Holm multiple testing correction was also applied (FDR(p) < 0.05).

For the probes showing significant differences in expression of mRNA between fibroblast strains from young and old strains, variation in expression between strains from different subjects was presented as a heatmap.

The Bonferroni-Holm data set was uploaded into the Ingenuity application [www.ingenuity.com]. Each probe identifier was mapped to its corresponding object/gene in Ingenuity's Knowledge Base. These molecules, called Network Eligible molecules, were overlaid onto a global molecular network developed from information contained in Ingenuity's Knowledge Base. Networks of Network Eligible Molecules were then algorithmically generated based on their connectivity. The Functional Analysis identified the biological functions and/or diseases that were most significant to the data set. Right-tailed Fisher's

exact test was used to calculate a p-value determining the probability that each biological function and/or disease assigned to that data set is due to chance alone. Canonical pathways analysis identified the pathways from the Ingenuity Pathways Analysis library of canonical pathways that were most significant to the data set. The significance of the association between the data set and the canonical pathway was measured in 2 ways: 1) A ratio of the number of molecules from the data set that map to the pathway divided by the total number of molecules that map to the canonical pathway is displayed. 2) Fisher's exact test was used to calculate a p-value determining the probability that the association between the genes in the dataset and the canonical pathway is explained by chance alone.

Gene Set Enrichment Analysis (GSEA; www.broad.mit.edu\gsea) (35;36) was applied for functional pathway analysis between comparative conditions. Probes from the microarray were collapsed into 17517 gene features and ordered by signal to noise ratio into a rank ordered list (L). For each gene set (S) an enrichment score (ES) is calculated which reflects the degree to which it is overrepresented at the extremes (top or bottom) of the entire ranked list L based on the Kolmogorov-Smirnov statistic. Briefly, the score is calculated by traversing the list L and increasing a running-sum statistic when a gene is encountered which is in S and decreasing it when genes are encountered which are not in S. The magnitude of the increment corresponds to the degree that the gene correlates to the phenotype. Statistical significance (nominal P-value) of the ES is determined by empirical phenotype-based permutation; specifically the phenotype labels are permuted and the ES of the gene set is recalculated to generate a null distribution for the ES. Nominal p-value is computed relative to this null distribution. Significance levels are then adjusted to account for multiple hypotheses testing first by normalizing the ES for each gene set to account for the size of the set (NES) and then by controlling the proportion of false positives by calculating the FDR corresponding to each NES. Gene sets were obtained from the Broad Institute Molecular Signatures Database.

All other analyses were performed with the software package SPSS 16.0.01 (SPSS Inc., Chicago, IL). Since the AU values from the Western blotting results were not normally distributed, they were normalised by log-transformation. Rotenone-induced effects were

analysed using linear mixed models (LMMs), adjusting for batches of experiments, repeat experiments and gender (and also age in case of offspring/partner comparison). Differences between groups (young/old, offspring/partner) in non-stressed and rotenone-stressed conditions were analysed using similar linear mixed models.

Results

Microarray analysis dependent on chronological age

SA-β-gal activity was measured in fibroblasts from young and old subjects under non-stressed and stressed conditions to assure that rotenone treatment for three days would increase levels of senescence, as previously observed (29). Six young subjects and six old subjects were randomly chosen (age: 23.1±1.6 [mean±SD] and 90.3±0.5 years, respectively, three males and three females for both young and old). All subjects were in good physical and mental condition and were able to come to the research institute. There was a significant increase in SA-β-gal activity in all fibroblast strains after three days of exposure to 0.6 μM rotenone (non-stressed: 2365±236 [MdFI in arbitrary units; mean±SE], rotenone: 4366±489, $p<0.001$). Furthermore, strains from old subjects showed a higher SA-β-gal activity under non-stressed conditions and a higher stress-induced increase in SA-β-gal activity (Supplemental table 2).

Gene expression profiles were generated using fibroblast strains from young and old subjects under non-stressed conditions and stressed for three hours and three days with rotenone. After quantile normalisation of the data, a linear regression model was used in conjunction with a Bonferroni-Holm multiple testing correction ($p<0.05$) to detect mRNAs that were differentially expressed between fibroblast strains from young and old subjects. A total of 215 out of 41094 probes were identified whose expression was significantly different between the fibroblast strains from young and old subjects (Supplemental table 1). Variation in expression between strains from different subjects was presented as a heatmap (Supplemental figure 1). These differences between young and old were present in the untreated samples as well as in the samples obtained after treatment with rotenone for three hours and after treatment with

rotenone for three days. The 215 differentially expressed probes could be mapped to 106 genes (Table 1).

Pathway analysis

To identify cellular pathways that could be responsible for the age-dependent changes in gene expression, Ingenuity Pathway Analysis was performed using all data and applying a Bonferroni-Holm cutoff to generate a target list for further study. The 215 probes could be mapped to 106 genes eligible for Ingenuity network analysis and 100 genes allowing function and canonical pathway analysis. Twelve over-represented gene networks were identified, with the most significant Ingenuity network containing p16 (CDKN2A) at its centre (Figure 1) and corresponding to the biological functions Tumour Morphology, Cell Cycle progression and Cellular Development. The biological function most significantly enriched in the 100 genes was Carbohydrate Metabolism. For the canonical pathway analysis Wnt/β-Catenin signaling was the most significantly enriched. The top 10 functions and canonical pathways derived from these analyses are shown in Figure 2.

To complement the Ingenuity analysis, a GSEA-based analysis was performed as this approach uses significance data across all the probes rather than a division of the list via a significant cutoff. When the data from old subjects were compared with that from young subjects, 446 of 967 gene sets were more highly expressed in the strains from the old subjects. Using a false discovery rate (FDR) cutoff of 0.25, the Glutamate Signaling Pathway appeared to be significantly enriched (nominal p-value: 0.006, FDR: 0.22, ES: 0.68, NES: -17.7) due to the differential regulation of the genes HOMER2, GRIA3, GRIN2B and GRIK2. In fibroblast strains from young subjects, 521 of 967 gene sets were more highly expressed when compared with strains from old subjects and 29 gene sets were significantly enriched at a FDR cutoff of 0.25 (Table 2). These gene sets were mainly involved in mitochondrial processes, the cytoskeleton (especially the machinery needed for mitosis) and RNA-processing.

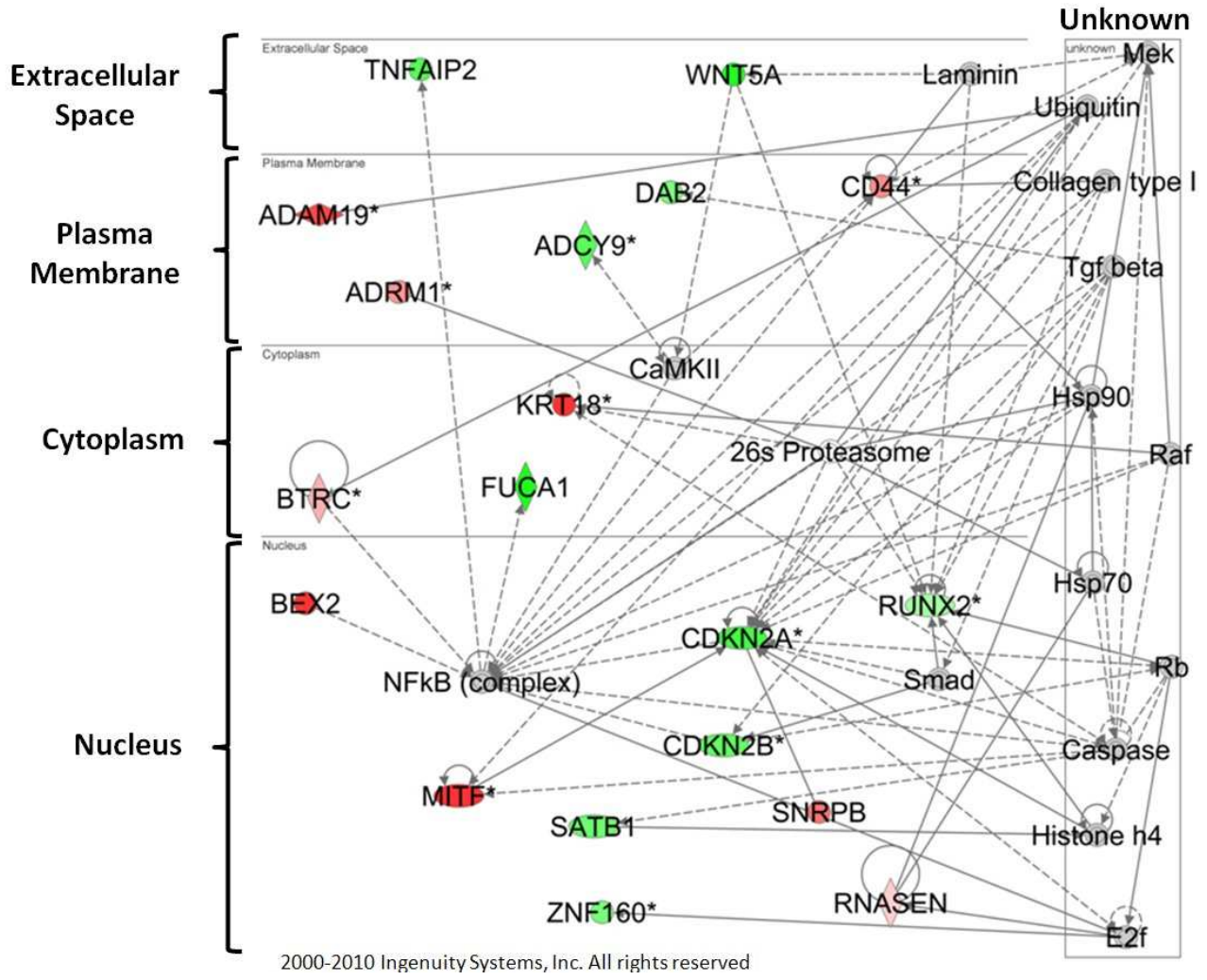

Figure 1. Top network generated by the use of Ingenuity Pathway Analysis (IPA), carried out on comparing young with old subjects with the Bonferroni-Holm cutoff applied ($p<0.05$). Molecules are represented as nodes, and the biological relationship between two nodes is represented as a line. The intensity of the node color indicates the degree of up- (red) or down- (green) regulation in fibroblast strains from young subjects. Nodes are displayed using various shapes that represent the functional class of the gene product (diamond: enzyme, horizontal oval: transcription factor, circle: other).

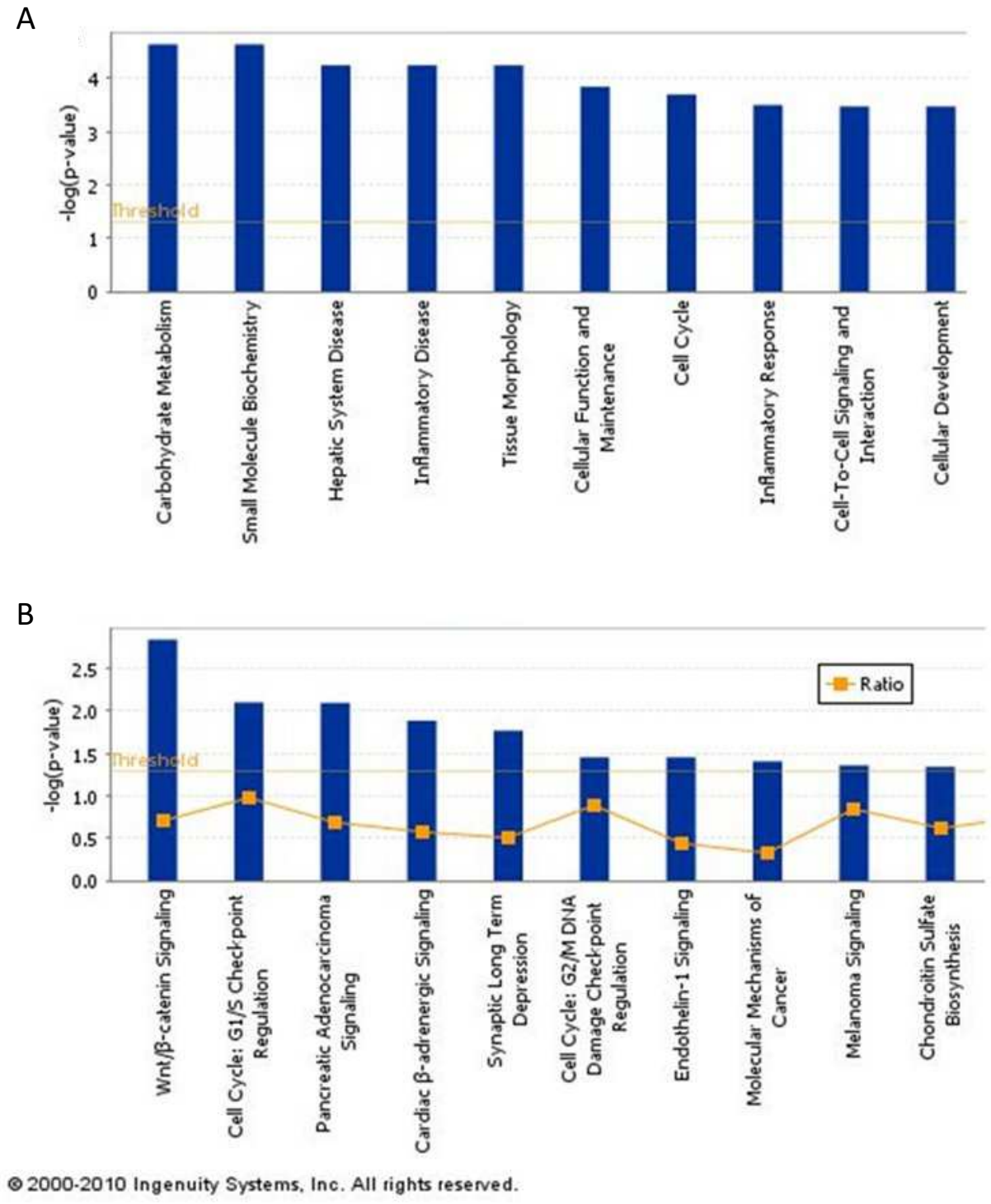

Figure 2. Ingenuity analysis. A, top 10 biological functions; B, top ten canonical pathways. Analysis was carried out on comparing young with old subjects with the Bonferroni-Holm cutoff applied ($p<0.05$). Ratio: expression in young/expression in old.

Table 1. List of genes to which the 215 differentially expressed probes could be mapped.

ID	Symbol	Entrez Gene Name	Location	Type(s)
A_23_P14515	ACOT4	acyl-CoA thioesterase 4	Cytoplasm	enzyme
A_23_P374082	ADAM19	ADAM metallopeptidase domain 19	Plasma Membrane	peptidase
A_24_P935103	ADCY9	adenylate cyclase 9	Plasma Membrane	enzyme
A_23_P68665	ADRM1	adhesion regulating molecule 1	Plasma Membrane	other
A_23_P317105	AKAP10	A kinase (PRKA) anchor protein 10	Cytoplasm	other
A_23_P158231	APBA2	amyloid beta (A4) precursor protein-binding, family A, member 2	Cytoplasm	transporter
A_23_P41166	B3GALNT1	beta-1,3-N-acetylgalactosaminyltransferase 1 (globoside blood group)	Cytoplasm	enzyme
A_23_P159952	BEX1	brain expressed, X-linked 1	Cytoplasm	other
A_23_P22735	BEX2	brain expressed X-linked 2	Nucleus	other
A_23_P35427	BTRC	beta-transducin repeat containing	Cytoplasm	enzyme
A_24_P201404	C11orf54	chromosome 11 open reading frame 54	Nucleus	other
A_32_P162183	C2	complement component 2	Extracellular Space	peptidase
A_23_P40315	C20orf12	chromosome 20 open reading frame 12	unknown	other
A_32_P142700	C22orf15	chromosome 22 open reading frame 15	unknown	other
A_32_P160972	C6orf115	chromosome 6 open reading frame 115	unknown	other
A_23_P73012	C9orf3	chromosome 9 open reading frame 3	Cytoplasm	peptidase
A_23_P155106	CCDC134	coiled-coil domain containing 134	unknown	other
A_23_P24870	CD44	CD44 molecule (Indian blood group)	Plasma Membrane	other
A_24_P42633	CDC42	cell division cycle 42 (GTP binding protein, 25kDa)	Cytoplasm	enzyme
A_23_P43484	CDKN2A	cyclin-dependent kinase inhibitor 2A (melanoma, p16, inhibits CDK4)	Nucleus	transcription regulator
A_24_P360674	CDKN2B	cyclin-dependent kinase inhibitor 2B (p15, inhibits CDK4)	Nucleus	transcription regulator
A_32_P99171	CHST11	carbohydrate (chondroitin 4) sulfotransferase 11	Cytoplasm	enzyme
A_24_P351435	CRBN	cereblon	Cytoplasm	enzyme
A_24_P76666	CSNK2A1	casein kinase 2, alpha 1 polypeptide	Cytoplasm	kinase
A_23_P202448	CXCL12	chemokine (C-X-C motif) ligand 12	Extracellular Space	cytokine
A_23_P257871	DAB2	disabled homolog 2, mitogen-responsive phosphoprotein (Drosophila)	Plasma Membrane	other
A_32_P230547	DOCK7	dedicator of cytokinesis 7	Plasma Membrane	other
A_23_P217079	DPM2	dolichyl-phosphate mannosyltransferase polypeptide 2, regulatory subunit	Cytoplasm	enzyme
A_23_P103232	DUSP23	dual specificity phosphatase 23	Cytoplasm	phosphatase
A_24_P375609	EIF5A	eukaryotic translation initiation factor 5A	Cytoplasm	translation regulator
A_23_P154806	EPB41L1	erythrocyte membrane protein band 4.1-like 1	Plasma Membrane	other
A_24_P166613	EPDR1	ependymin related protein 1 (zebrafish)	Nucleus	other
A_23_P71981	ERAL1	Era G-protein-like 1 (E. coli)	Cytoplasm	other
A_24_P314451	F8	coagulation factor VIII, procoagulant component	Extracellular Space	other
A_32_P39093	FAM108C1	family with sequence similarity 108, member C1	unknown	enzyme
A_23_P167599	FAM134B	family with sequence similarity 134, member B	Cytoplasm	other
A_24_P38316	FOXP2	forkhead box P2	Nucleus	transcription

				regulator
A_23_P11543	FUCA1	fucosidase, alpha-L- 1, tissue	Cytoplasm	enzyme
A_23_P25964	GALC	galactosylceramidase	Cytoplasm	enzyme
A_24_P217489	GLRB	glycine receptor, beta	Plasma Membrane	ion channel
A_23_P416581	GNAZ	guanine nucleotide binding protein (G protein), alpha z polypeptide	Plasma Membrane	enzyme
A_32_P132317	GPR155	G protein-coupled receptor 155	Plasma Membrane	G-protein coupled receptor
A_23_P139864	GSG1	germ cell associated 1	Cytoplasm	other
A_23_P98431	HMBS	hydroxymethylbilane synthase	Cytoplasm	enzyme
A_32_P50924	HNRNPA1L2	heterogeneous nuclear ribonucleoprotein A1-like 2	Nucleus	other
A_23_P170687	HSPBP1	HSPA (heat shock 70kDa) binding protein, cytoplasmic cochaperone 1	unknown	other
A_23_P48513	IFI27	interferon, alpha-inducible protein 27	Cytoplasm	other
A_23_P343954	IGF2BP1	insulin-like growth factor 2 mRNA binding protein 1	Cytoplasm	translation regulator
A_23_P19987	IGF2BP3	insulin-like growth factor 2 mRNA binding protein 3	Cytoplasm	translation regulator
A_23_P257956	ILF2	interleukin enhancer binding factor 2, 45kDa	Nucleus	transcription regulator
A_32_P87872	IMMP2L	IMP2 inner mitochondrial membrane peptidase-like (S. cerevisiae)	Cytoplasm	peptidase
A_23_P19852	IQCE	IQ motif containing E	Cytoplasm	other
A_23_P324523	IQCK	IQ motif containing K	unknown	other
A_23_P112201	KDM4C	lysine (K)-specific demethylase 4C	Nucleus	other
A_32_P151544	KRT18	keratin 18	Cytoplasm	other
A_23_P93750	LSM5	LSM5 homolog, U6 small nuclear RNA associated (S. cerevisiae)	Cytoplasm	other
A_24_P314640	MDGA1	MAM domain containing glycosylphosphatidylinositol anchor 1	Plasma Membrane	other
A_23_P61945	MITF	microphthalmia-associated transcription factor	Nucleus	transcription regulator
A_23_P135474	MRPL37	mitochondrial ribosomal protein L37	Cytoplasm	enzyme
A_32_P117170	NAPEPLD	N-acyl phosphatidylethanolamine phospholipase D	Cytoplasm	enzyme
A_24_P367752	NDST1	N-deacetylase/N-sulfotransferase (heparan glucosaminyl) 1	Cytoplasm	enzyme
A_23_P300600	NEFH	neurofilament, heavy polypeptide	Cytoplasm	other
A_23_P91328	NOP56	NOP56 ribonucleoprotein homolog (yeast)	Nucleus	other
A_23_P59547	NT5C3	5'-nucleotidase, cytosolic III	Cytoplasm	phosphatase
A_24_P360206	PCDHA11	protocadherin alpha 11	Plasma Membrane	other
A_32_P116857	PDE11A	phosphodiesterase 11A	Cytoplasm	enzyme
A_23_P411723	PLAG1	pleiomorphic adenoma gene 1	Nucleus	transcription regulator
A_23_P17914	PNPLA3	patatin-like phospholipase domain containing 3	Cytoplasm	enzyme
A_24_P570049	PPARA	peroxisome proliferator-activated receptor alpha	Nucleus	ligand-dependent nuclear receptor
A_23_P60458	PPP2R4	protein phosphatase 2A activator, regulatory subunit 4	Cytoplasm	phosphatase
A_23_P146554	PTGDS	prostaglandin D2 synthase 21kDa (brain)	Cytoplasm	enzyme
A_23_P203729	RAB6A	RAB6A, member RAS oncogene family	Cytoplasm	enzyme
A_23_P166087	RASSF2	Ras association (RalGDS/AF-6) domain family member 2	Nucleus	other
A_23_P9056	RB1CC1	RB1-inducible coiled-coil 1	Nucleus	other

A_23_P133596	DROSHA	drosha, ribonuclease type III	Nucleus	enzyme
A_24_P199500	RNF2	ring finger protein 2	Nucleus	transcription regulator
A_23_P6802	RRP9	ribosomal RNA processing 9, small subunit (SSU) processome component, homolog (yeast)	Nucleus	other
A_32_P161762	RUNX2	runt-related transcription factor 2	Nucleus	transcription regulator
A_23_P259741	SATB1	SATB homeobox 1	Nucleus	transcription regulator
A_23_P152548	SCPEP1	serine carboxypeptidase 1	Cytoplasm	peptidase
A_23_P150092	SEPHS1	selenophosphate synthetase 1	unknown	enzyme
A_23_P106299	SERF2	small EDRK-rich factor 2	unknown	other
A_32_P4595	SGCD	sarcoglycan, delta (35kDa dystrophin-associated glycoprotein)	Cytoplasm	other
A_23_P139260	SLC22A18	solute carrier family 22, member 18	Plasma Membrane	transporter
A_23_P436179	SLC25A5	solute carrier family 25 (mitochondrial carrier; adenine nucleotide translocator), member 5	Cytoplasm	transporter
A_23_P24345	SLC39A13	solute carrier family 39 (zinc transporter), member 13	unknown	transporter
A_23_P50167	SLC39A6	solute carrier family 39 (zinc transporter), member 6	Plasma Membrane	transporter
A_23_P154675	SNRPB	small nuclear ribonucleoprotein polypeptides B and B1	Nucleus	other
A_32_P43711	SOCS7	suppressor of cytokine signaling 7	Cytoplasm	other
A_32_P89755	SSR1	signal sequence receptor, alpha	Cytoplasm	other
A_23_P36076	SSRP1	structure specific recognition protein 1	Nucleus	other
A_23_P43164	SULF1	sulfatase 1	Cytoplasm	enzyme
A_23_P96965	SYNC	syncoilin, intermediate filament protein	Cytoplasm	other
A_32_P66881	TLR4	toll-like receptor 4	Plasma Membrane	transmembrane receptor
A_23_P103282	TMEM59	transmembrane protein 59	Plasma Membrane	other
A_23_P216522	TMEM8B	transmembrane protein 8B	Plasma Membrane	other
A_23_P421423	TNFAIP2	tumor necrosis factor, alpha-induced protein 2	Extracellular Space	other
A_23_P363344	TPM1 (includes EG:22003)	tropomyosin 1 (alpha)	Cytoplasm	other
A_23_P16683	TRMT1	TRM1 tRNA methyltransferase 1 homolog (S. cerevisiae)	unknown	enzyme
A_23_P79510	VPS24	vacuolar protein sorting 24 homolog (S. cerevisiae)	Cytoplasm	other
A_23_P141394	WIPI1	WD repeat domain, phosphoinositide interacting 1	Cytoplasm	other
A_23_P211926	WNT5A	wingless-type MMTV integration site family, member 5A	Extracellular Space	cytokine
A_32_P34516	XKR6	XK, Kell blood group complex subunit-related family, member 6	unknown	other
A_23_P134527	YKT6	YKT6 v-SNARE homolog (S. cerevisiae)	Cytoplasm	enzyme

Table 2. Gene sets more higly expressed in fibroblast strains from young subjects when compared with strains from old subjects, and significantly enriched at FDR<0.25, identified by GSEA.

Gene set	p	FDR	ES	NES
MITOCHONDRIAL_INNER_MEMBRANE	0.010	0.163	-0.58	-17.72
SPINDLE	0.000	0.217	-0.85	-16.00
NUCLEAR_EXPORT	0.024	0.218	-0.54	-15.76
PORE_COMPLEX	0.027	0.220	-0.63	-16.04
MICROTUBULE_ORGANIZING_CENTER	0.010	0.225	-0.58	-15.81
SPINDLE_POLE	0.004	0.226	-0.84	-15.77
SPLICEOSOME	0.048	0.228	-0.55	-15.92
MITOCHONDRIAL_PART	0.054	0.229	-0.44	-16.05
RNA_DEPENDENT_ATPASE_ACTIVITY	0.008	0.230	-0.71	-16.15
MITOCHONDRIAL_RIBOSOME	0.052	0.231	-0.62	-1.62
MICROTUBULE_ORGANIZING_CENTER_PART	0.024	0.231	-0.65	-15.82
RNA_BINDING	0.017	0.233	-0.36	-15.86
MITOCHONDRIAL_MEMBRANE	0.008	0.235	-0.52	-17.75
MICROTUBULE_CYTOSKELETON	0.020	0.235	-0.57	-1.55
NUCLEOLUS	0.008	0.235	-0.48	-16.61
SMALL_NUCLEAR_RIBONUCLEOPROTEIN_COMPLEX	0.012	0.239	-0.66	-17.21
MITOCHONDRIAL_MEMBRANE_PART	0.076	0.239	-0.52	-15.51
CYTOSKELETAL_PART	0.018	0.239	-0.52	-15.48
MITOCHONDRIAL_ENVELOPE	0.039	0.240	-0.46	-1.63
NUCLEAR_LUMEN	0.010	0.240	-0.41	-15.31
VIRAL_REPRODUCTIVE_PROCESS	0.006	0.242	-0.64	-16.05
ORGANELLE_INNER_MEMBRANE	0.020	0.244	-0.53	-17.03
FEMALE_GAMETE_GENERATION	0.029	0.244	-0.72	-15.32
RNA_HELICASE_ACTIVITY	0.013	0.246	-0.68	-16.42
VIRAL_REPRODUCTION	0.011	0.246	-0.59	-15.40
RIBOSOMAL_SUBUNIT	0.063	0.247	-0.63	-15.51
ORGANELLAR_RIBOSOME	0.052	0.247	-0.62	-1.62
ATP_DEPENDENT_HELICASE_ACTIVITY	0.004	0.247	-0.69	-16.67
TRANSLATION_FACTOR_ACTIVITY__NUCLEIC_ACID_BINDING	0.044	0.248	-0.53	-15.36

FDR: false discovery rate, ES: enrichment score, NES: normalised enrichment score

p16

An expression probe corresponding to p16 was the most significantly differentially expressed probe between fibroblast strains from young and old subjects, being higher in strains from old subjects. Rotenone-treatment resulted in decreases in p16 mRNA expression after three hours and even more so after three days which were similar for fibroblast strains from young and old subjects, i.e. there was no significant rotenone-age interaction. This was validated by qPCR (non-stressed=1, fold change 3 hours rotenone [mean±SE]: 0.74±0.04, fold change 3 days rotenone: 0.67±0.04, $p<0.001$). For each condition, p16 mRNA levels were found to be higher in fibroblast strains from old subjects (Supplemental table 2). To verify these results, we performed a replication experiment on fibroblast strains from a new set of ten young and ten old subjects (age: 25.5±1.8 [mean±SD] and 90.2±0.3 years). To assess the rotenone-induced stress response, levels of reactive oxygen species (ROS [MdFI in arbitrary units] non-stressed: 1580±70 [mean±SE], rotenone: 2181±124, $p<0.001$) and SA-β-gal activity ([MdFI in arbitrary units] non-stressed: 2793±278, rotenone: 4278±330, $p<0.001$) were measured. There was no difference in SA-β-gal activity between strains from young and old subjects, but strains from old subjects did show a greater rotenone-induced increase in SA-β-gal activity (Supplemental table 2). Under non-stressed conditions ROS levels were higher in strains from old subjects (MdFI in arbitrary units, young: 1500±150, old: 1656±148, $p=0.027$), but there were no differences in rotenone-induced increases. p16 was measured by qPCR, Western blotting and immunocytochemistry (ICC). Consistent with the microarray experiments, p16 mRNA expression decreased (non-stressed=1, rotenone: 0.74±0.04, $p<0.001$). Under non-stressed conditions, fibroblast strains from old subjects showed significantly lower levels of p16 mRNA when compared with strains of young subjects (Supplemental table 2), contrary to the microarray results of the microarray experiment. Under stressed conditions there was no difference in p16 mRNA expression or protein levels. Western blotting demonstrated neither rotenone-induced changes in p16 protein levels, nor any differences between strains from young and old subjects. ICC showed rotenone-induced increases in p16 positive fibroblasts (Non-stressed: 2.40±0.31%, rotenone: 7.02±0.72%, $p<0.001$). Under non-stressed conditions percentages of p16-positive fibroblasts were higher for strains from old subjects when compared with strains from young subjects (young:

+1.39±0.31%, old: +3.05±0.31%, p<0.001), as were rotenone-induced increases in p16 positive percentages (young: +3.43±0.65%, old: +5.08±0.65%, p=0.060).

Discussion

In this study we addressed which pathways could be responsible for the reported differences in senescence and apoptosis between fibroblast strains from young and old subjects (25;37) using microarray methodology. Age-dependent differences were found in pathways involved in carbohydrate metabolism, Wnt/β-catenin signalling, the cytoskeleton, cell cycle, RNA-processing and mitochondrial function. No significant rotenone-age interactions were detected in this analysis indicating that the differences with age in mRNA levels were generally similar in stressed and non-stressed conditions.

Ingenuity analysis

Ingenuity analysis identified carbohydrate metabolism as the biological function that was most differentially expressed between strains from young and old subjects. The most significant pathway within this function was modification of glycosaminoglycans (GAGs), which are important components of the extracellular matrix (ECM). In support of this finding, it has been reported that physiological aging is associated with ECM remodeling, reflected by plasma GAGs concentrations (38). Genes involved in carbohydrate metabolism identified by Ingenuity were, amongst others, CD44, CXCL12 and TLR4. CD44 is a cell-surface glycoprotein important for cell-cell interactions, cell adhesion and migration (39;40). In aged fibroblasts, TGF-1-induced association between CD44 and EGF-R is lost with resultant suppression of ERK1/2 activation (41) and this might explain the lower CD44-expression in fibroblast strains from old subjects that we observed. In addition, CD44 is a receptor for hyaluran (HA), which is an important component of the ECM. HA acts through TLR4 and CD44 to stimulate an immune response against the septic response (42). Lower TLR4 activity has also been linked to reduced inflammatory response and successful aging (43), consistent with the higher TLR4-expression in fibroblast strains from old subjects observed in

the study reported here. CXCL12/SDF-1 is a chemotactic cytokine involved in cell motility (44) and showed lower expression in fibroblast strains from old subjects, correlating well with the decreased expression with age reported in animal models (45). Taken together, these results suggest that differences in cell to cell signaling might explain the differential regulation of carbohydrate metabolism between fibroblast strains from young and old subjects.

The most significant canonical pathway identified by the Ingenuity analysis was the Wnt/β-catenin pathway, which is frequently deregulated in cancer (46;47) and consists of, amongst others, the genes B-TRCP, CK2, CDKN2A (or p14/p16: see below) and WNT5A. WNT5A-expression was higher in fibroblast strains from old subjects, consistent with reduced cell proliferation in fibroblast strains from old subjects (25) and age-dependent increased WNT5A-expression reported for animal models (48). In support of this, the top Ingenuity network indicated reduced cell proliferation in fibroblast strains from old subjects via the increases found in p15, p16 and RUNX2 mRNA. However, the expression levels of some genes were opposite to that expected. For example, B-TRCP is involved in ubiquitination and degradation of β-catenin which, as a consequence, leads to cell cycle arrest (49) and CK2 is activated by Wnt/β-catenin signalling (50). We found lower B-TRCP and CK2 expression in fibroblast strains from old subjects, suggesting increased cell proliferation. Thus, although the Ingenuity analysis indicated reduced cellular proliferation in fibroblast strains from old subjects, some contradictory findings warrant further pathway analysis to validate the findings.

GSEA analysis

GSEA pathway analysis resulted in gene sets such as spindle, spindle pole and microtubule organizing centre showing lower expression in fibroblast strains from old subjects, supporting the view that there was inhibition of the cell cycle in fibroblast strains from the old subjects. In addition, there was an increased activity of pathways linked to RNA processing in the young strains, consistent with the idea that with cellular aging (senescence) the expression of many genes required for the cell cycle decrease (51). Indeed, fewer senescent fibroblasts are observed in strains from young subjects (25). Combined with the Ingenuity analysis, these

results suggest a reduced cellular proliferation rate in fibroblast strains from old subjects, as we indeed showed recently (37).

Mitochondrial function was also detected by the GSEA analysis. This was striking because rotenone binds to the electron transport chain in mitochondria, disrupting the production of ATP (52). Our previous results demonstrated that rotenone treatment exacerbated differences in the number of fibroblasts entering cellular senescence and apoptosis between strains from young and old subjects (25). Thus, as mitochondrial membrane potential is impaired in fibroblasts from old subjects (53), rotenone insult could lead to greater ROS production in the fibroblasts from the old subjects and consequently more cellular senescence.

GSEA analysis also identified the Glutamate Signaling Pathway gene set as the most differentially upregulated pathway in the fibroblast strains from the old subjects. Although fibroblasts are known to utilize glutamate signaling (54), very little is known about the role glutamate signaling plays in fibroblast function. These results are the first to indicate that glutamate signaling is upregulated with age in skin fibroblasts and the consequences of these changes on fibroblast function now requires further examination.

Boraldi et al. (55) also compared fibroblast strains from young and old subjects (ex vivo aging model) at early and late CPDs (in vitro aging model). While showing the majority of differences, like stress response, endoplasmic reticulum and cell membrane compartments and post-translational protein modifications, for in vitro aging, they did not observe many differences dependent on the age of subjects. It must be noted, though, that they used only three strains per age group. Although the effect was more pronounced in in vitro aging, they did find that deterioration of the redox balance depended on the subjects' age, consistent with the difference in expression of genes involved in mitochondrial function that reported here. Furthermore, elastin and fibulin-5 expression, both important ECM components, were differently expressed in cultures between fibroblast strains from young and old donors, consistent with the different expression of genes involved in ECM remodeling, cell-cell interactions and cell adhesion reported here.

p16

The gene most differentially expressed between fibroblast strains from young and old subjects was p16 and this microarray finding was confirmed by qPCR. p16 is regarded as a robust marker for cellular aging and senescence (2;56) and increasing numbers of p16-positive cells can indeed be found in mitotic aging of aging primates (57;58). We hypothesized that increased numbers of senescent cells (SA-β-gal activity) would be paralleled by p16 mRNA after rotenone-treatment. However, a decrease was observed in both the microarray experiment and the replication experiment. Furthermore, Western blot analyses could not show rotenone-induced differences in p16 protein levels whereas ICC did show rotenone-induced increased numbers of p16-positive fibroblasts. Thus, p16 mRNA levels were not reflected by p16 protein levels as measured by Western blot analysis and ICC.

Regulation of p16 activity can occur at different levels: transcription, mRNA stability, translation and protein stability. p16 mRNA stability is controlled by genes regulating the degradation of p16 mRNA which are down-regulated in late passage fibroblasts (59;60). In addition, p16 protein levels can increase in the absence of changes to p16 mRNA levels via changes to p16 protein stability (61;62). Thus, in senescent cells p16 mRNA and protein levels are likely to be stable whereas p16 protein stabilization rather than increased p16 mRNA levels could be responsible for non-senescent cells entering cell arrest. Another explanation could be that the microarray and qPCR probes both corresponded to the 3' end of the gene which is common to at least two gene transcripts (p14 and p16) whereas the proteins transcribed from the locus are unique in sequence (63). Thus, differential regulation of the different transcripts between the two experiments might well dissociate any concordance that actually exists between p16 mRNA and protein levels. The discrepancies between ICC and Western blotting could be explained by the fact that the ICC method scores each fibroblast dichotomously, while Western blotting measures the average level of all fibroblasts, underestimating the p16 positivity of some fibroblasts and overestimating the negativity of other fibroblasts, resulting in no average change.

In the microarray experiments the fibroblast strains from the old subjects showed higher levels of p16 mRNA expression for all three conditions (non-stressed, 3 hours and 3 days rotenone) consistent with increasing numbers of p16-positive fibroblasts in aging primates (57;64). No differences in the rotenone-induced fold changes in p16 mRNA expression were detected. In contrast to the microarray experiments the replication experiments showed lower expression of p16 mRNA in strains from old subjects (non-stressed) and rotenone induced a smaller decrease in p16 mRNA expression in these strains. The consistency of the p16 mRNA results across strains within each experiment, and the concordance of the ICC results across experiments indicated that the cause of this difference was technical in nature and specific to the mRNA. For example, a higher seeding density (to maximize mRNA yield) used for the microarray experiment compared with the replication experiments could have lead to differential regulation of p16 expression (65). Alternatively, changes to the expression of the housekeeping gene used in the qPCR experiments could have resulted in different qPCR results. Further detailed work investigating differences in p16 mRNA between fibroblast strains from young and old subjects, along with epistatic control of p16 mRNA levels is now required. However, as the most accurate reflection of p16 function, the ICC results reflected the gene array pathway analyses, the SA-β-gal activity and previous reported work (29) that cell cycle arrest is higher in fibroblasts strains from old subjects compared with young subjects. These results suggest that mRNA is not necessarily the best marker of p16 and ICC might be a better candidate.

In conclusion, from the microarray analyses emerged pathways involved in carbohydrate metabolism, cell cycle, mitochondrial function, glutamate signaling and RNA processing. The cell cycle inhibitor p16, involved in senescence, was the most significantly differentially expressed mRNA between fibroblast strains from young and old subjects. The discrepancies between the microarray experiments and the replication experiments could be explained by non-representative strain selection and/or technical issues regarding seeding density. Future work with higher numbers of fibroblast strains will need to identify common pathways between the contrast in chronological age and biological age (e.g. familial longevity). These pathways might then be manipulated, resulting in biologically old cells becoming biologically younger, i.e. resemble chronologically cells.

References

(1) Campisi J. Cellular senescence and apoptosis: how cellular responses might influence aging phenotypes. Exp Gerontol 2003;38:5-11.

(2) Ben-Porath I, Weinberg RA. The signals and pathways activating cellular senescence. Int J Biochem Cell Biol 2005;37:961-976.

(3) Han E, Hilsenbeck SG, Richardson A, Nelson JF. cDNA expression arrays reveal incomplete reversal of age-related changes in gene expression by calorie restriction. Mech Ageing Dev 2000;20;115:157-174.

(4) Prolla TA. DNA microarray analysis of the aging brain. Chem Senses 2002;27:299-306.

(5) Crott JW, Choi SW, Ordovas JM, Ditelberg JS, Mason JB. Effects of dietary folate and aging on gene expression in the colonic mucosa of rats: implications for carcinogenesis. Carcinogenesis 2004;25:69-76.

(6) Ida H, Boylan SA, Weigel AL, Hjelmeland LM. Age-related changes in the transcriptional profile of mouse RPE/choroid. Physiol Genomics 2003;15:258-262.

(7) Lluel P, Palea S, Ribiere P, Barras M, Teillet L, Corman B. Increased adrenergic contractility and decreased mRNA expression of NOS III in aging rat urinary bladders. Fundam Clin Pharmacol 2003;17:633-641.

(8) Vazquez-Padron RI, Lasko D, Li S, Louis L, Pestana IA, Pang M, Liotta C, Fornoni A, Aitouche A, Pham SM. Aging exacerbates neointimal formation, and increases proliferation and reduces susceptibility to apoptosis of vascular smooth muscle cells in mice. J Vasc Surg 2004;40:1199-1207.

(9) Edwards MG, Anderson RM, Yuan M, Kendziorski CM, Weindruch R, Prolla TA. Gene expression profiling of aging reveals activation of a p53-mediated transcriptional program. BMC Genomics 2007;8:80.:80.

(10) Meyer RA, Jr., Desai BR, Heiner DE, Fiechtl J, Porter S, Meyer MH. Young, adult, and old rats have similar changes in mRNA expression of many skeletal genes after fracture despite delayed healing with age. J Orthop Res 2006;24:1933-1944.

(11) Edwards MG, Sarkar D, Klopp R, Morrow JD, Weindruch R, Prolla TA. Impairment of the transcriptional responses to oxidative stress in the heart of aged C57BL/6 mice. Ann N Y Acad Sci 2004;1019:85-95.:85-95.

(12) Tollet-Egnell P, Parini P, Stahlberg N, Lonnstedt I, Lee NH, Rudling M, Flores-Morales A, Norstedt G. Growth hormone-mediated alteration of fuel metabolism in the aged rat as determined from transcript profiles. Physiol Genomics 2004;16:261-267.

(13) Park SK, Prolla TA. Gene expression profiling studies of aging in cardiac and skeletal muscles. Cardiovasc Res 2005;66:205-212.

(14) Kyng KJ, May A, Kolvraa S, Bohr VA. Gene expression profiling in Werner syndrome closely resembles that of normal aging. P Natl Acad Sci USA 2003;100:12259-12264.

(15) Geigl JB, Langer S, Barwisch S, Pfleghaar K, Lederer G, Speicher MR. Analysis of gene expression patterns and chromosomal changes associated with aging. Cancer Res 2004;64:8550-8557.

(16) Melk A, Mansfield ES, Hsieh SC, Hernandez-Boussard T, Grimm P, Rayner DC, Halloran PF, Sarwal MM. Transcriptional analysis of the molecular basis of human kidney aging using cDNA microarray profiling. Kidney Int 2005;68:2667-2679.

(17) Lazuardi L, Herndler-Brandstetter D, Brunner S, Laschober GT, Lepperdinger G, Grubeck-Loebenstein B. Microarray analysis reveals similarity between CD8+CD28- T cells from young and elderly persons, but not of CD8+CD28+ T cells. Biogerontology 2009;10:191-202.

(18) Welle S, Brooks A, Thornton CA. Senescence-related changes in gene expression in muscle: similarities and differences between mice and men. Physiol Genomics 2001;5:67-73.

(19) Hazane-Puch F, Bonnet M, Valenti K, Schnebert S, Kurfurst R, Favier A, Sauvaigo S. Study of fibroblast gene expression in response to oxidative stress induced by hydrogen peroxide or UVA with skin aging. Eur J Dermatol 2010;20:308-320.

(20) Lener T, Moll PR, Rinnerthaler M, Bauer J, Aberger F, Richter K. Expression profiling of aging in the human skin. Exp Gerontol 2006;41:387-397.

(21) Ma H, Li R, Zhang Z, Tong T. mRNA level of alpha-2-macroglobulin as an aging biomarker of human fibroblasts in culture. Exp Gerontol 2004;39:415-421.

(22) Welle S, Brooks AI, Delehanty JM, Needler N, Bhatt K, Shah B, Thornton CA. Skeletal muscle gene expression profiles in 20-29 year old and 65-71 year old women. Exp Gerontol 2004;39:369-377.

(23) Welle S, Brooks AI, Delehanty JM, Needler N, Thornton CA. Gene expression profile of aging in human muscle. Physiol Genomics 2003;14:149-159.

(24) Thomas RP, Guigneaux M, Wood T, Evers BM. Age-associated changes in gene expression patterns in the liver. J Gastrointest Surg 2002;6:445-453.

(25) Dekker P, Maier AB, van HD, de Koning-Treurniet C, Blom J, Dirks RW, Tanke HJ, Westendorp RG. Stress-induced responses of human skin fibroblasts in vitro reflect human longevity. Aging Cell 2009;8:595-603.

(26) Bootsma-van der Wiel A, Gussekloo J, de Craen AJM, van Exel E, Bloem BR, Westendorp RGJ. Common chronic diseases and general impairments as determinants of walking disability in the oldest-old population. J Am Geriatr Soc 2002;50:1405-1410.

(27) Maier AB, le Cessie S, Koning-Treurniet C, Blom J, Westendorp RG, van Heemst D. Persistence of high-replicative capacity in cultured fibroblasts from nonagenarians. Aging Cell 2007;6:27-33.

(28) Li N, Ragheb K, Lawler G, Sturgis J, Rajwa B, Melendez JA, Robinson JP. Mitochondrial complex I inhibitor rotenone induces apoptosis through enhancing mitochondrial reactive oxygen species production. J Biol Chem 2003;278:8516-8525.

(29) Noppe G, Dekker P, Koning-Treurniet C, Blom J, van Heemst D, Dirks RJ, Tanke HJ, Westendorp RG, Maier AB. Rapid flow cytometric method for measuring Senescence Associated â-galactosidase activity in human fibroblasts. Cytometry A 2009;75:910-916.

(30) Edgar R, Domrachev M, Lash AE. Gene Expression Omnibus: NCBI gene expression and hybridization array data repository. Nucleic Acids Res 2002;30:207-210.

(31) Barrett T, Troup DB, Wilhite SE, Ledoux P, Evangelista C, Kim IF, Tomashevsky M, Marshall KA, Phillippy KH, Sherman PM, Muertter RN, Holko M, Ayanbule O, Yefanov A, Soboleva A. NCBI GEO: archive for functional genomics data sets--10 years on. Nucleic Acids Res 2011;39:D1005-D1010.

(32) Ihaka R, Gentleman R. R: a language for data analysis and graphics. J Comput Graph Stat 1996;5:299-314.

(33) Ritchie ME, Silver J, Oshlack A, Holmes M, Diyagama D, Holloway A, Smyth GK. A comparison of background correction methods for two-colour microarrays. Bioinformatics 2007;23:2700-2707.

(34) Smyth GK. Linear models and empirical bayes methods for assessing differential expression in microarray experiments. Stat Appl Genet Mol Biol 2004;3:Article3.

(35) Subramanian A, Tamayo P, Mootha VK, Mukherjee S, Ebert BL, Gillette MA, Paulovich A, Pomeroy SL, Golub TR, Lander ES, Mesirov JP. Gene set enrichment analysis: a knowledge-based approach for interpreting genome-wide expression profiles. P Natl Acad Sci USA 2005;102:15545-15550.

(36) Mootha VK, Lindgren CM, Eriksson KF, Subramanian A, Sihag S, Lehar J, Puigserver P, Carlsson E, Ridderstrale M, Laurila E, Houstis N, Daly MJ, Patterson N, Mesirov JP, Golub TR, Tamayo P, Spiegelman B, Lander ES, Hirschhorn JN, Altshuler D, Groop LC. PGC-1alpha-responsive genes involved in oxidative phosphorylation are coordinately downregulated in human diabetes. Nat Genet 2003;34:267-273.

(37) Dekker P, van Baalen LM, Dirks RW, Slagboom PE, van Heemst D, Tanke HJ, Westendorp RGJ, Maier AB. Chronic inhibition of the respiratory chain differentially affects fibroblast strains from young and old subjects. J Gerontol A Biol Sci Med Sci 2011 Nov 10 [Epub ahead of print].

(38) Komosinska-Vassev K, Olczyk P, Winsz-Szczotka K, Klimek K, Olczyk K. Age- and gender-dependent changes in circulating concentrations of tumor necrosis factor-alpha, soluble tumor necrosis factor receptor-1 and sulfated glycosaminoglycan in healthy people. Clin Chem Lab Med 2011;49:121-127.

(39) Naor D, Nedvetzki S. CD44 in rheumatoid arthritis. Arthritis Res Ther 2003;5:105-115.

(40) Robert L, Robert AM, Renard G. Biological effects of hyaluronan in connective tissues, eye, skin, venous wall. Role in aging. Pathol Biol (Paris) 2010;58:187-198.

(41) Simpson RM, Wells A, Thomas D, Stephens P, Steadman R, Phillips A. Aging fibroblasts resist phenotypic maturation because of impaired hyaluronan-dependent CD44/epidermal growth factor receptor signaling. Am J Pathol 2010;176:1215-1228.

(42) Muto J, Yamasaki K, Taylor KR, Gallo RL. Engagement of CD44 by hyaluronan suppresses TLR4 signaling and the septic response to LPS. Mol Immunol 2009;47:449-456.

(43) Balistreri CR, Candore G, Listi F, Fazio T, Gangi S, Incalcaterra E, Caruso M, Vecchi ML, Lio D, Caruso C. Role of TLR4 polymorphisms in inflammatory responses: implications for unsuccessful aging. Ann N Y Acad Sci 2007;1119:203-7.:203-207.

(44) Bleul CC, Fuhlbrigge RC, Casasnovas JM, Aiuti A, Springer TA. A highly efficacious lymphocyte chemoattractant, stromal cell-derived factor 1 (SDF-1). J Exp Med 1996;184:1101-1109.

(45) Loh SA, Chang EI, Galvez MG, Thangarajah H, El-ftesi S, Vial IN, Lin DA, Gurtner GC. SDF-1 alpha expression during wound healing in the aged is HIF dependent. Plast Reconstr Surg 2009;123:65S-75S.

(46) Fodde R, Brabletz T. Wnt/beta-catenin signaling in cancer stemness and malignant behavior. Curr Opin Cell Biol 2007;19:150-158.

(47) Dominguez I, Sonenshein GE, Seldin DC. Protein kinase CK2 in health and disease: CK2 and its role in Wnt and NF-kappaB signaling: linking development and cancer. Cell Mol Life Sci 2009;66:1850-1857.

(48) Rauner M, Sipos W, Pietschmann P. Age-dependent Wnt gene expression in bone and during the course of osteoblast differentiation. Age (Dordr) 2008;30:273-282.

(49) Sahasrabuddhe AA, Dimri M, Bommi PV, Dimri GP. Beta TrCP regulates BMI1 protein turnover via ubiquitination and degradation. Cell Cycle 2011;10.

(50) Gao Y, Wang HY. Casein kinase 2 Is activated and essential for Wnt/beta-catenin signaling. J Biol Chem 2006;281:18394-18400.

(51) Chen KY. Transcription factors and the down-regulation of G1/S boundary genes in human diploid fibroblasts during senescence. Front Biosci 1997;2:d417-26.:d417-d426.

(52) Koopman WJ, Nijtmans LG, Dieteren CE, Roestenberg P, Valsecchi F, Smeitink JA, Willems PH. Mammalian mitochondrial complex I: biogenesis, regulation, and reactive oxygen species generation. Antioxid Redox Signal 2010;12:1431-1470.

(53) Koziel R, Greussing R, Maier AB, Declercq L, Jansen-Durr P. Functional interplay between mitochondrial and proteasome activity in skin aging. J Invest Dermatol 2011;131:594-603.

(54) Zeng Y, Lv X, Zeng S, Shi J. Activity-dependent neuronal control of gap-junctional communication in fibroblasts. Brain Res 2009;1280:13-22.

(55) Boraldi F, Annovi G, Tiozzo R, Sommer P, Quaglino D. Comparison of ex vivo and in vitro human fibroblast ageing models. Mech Ageing Dev 2010;131:625-635..

(56) Campisi J, d'Adda di Fagagna F. Cellular senescence: when bad things happen to good cells. Nat Rev Mol Cell Biol 2007;8:729-740.

(57) Jeyapalan JC, Ferreira M, Sedivy JA, Herbig U. Accumulation of senescent cells in mitotic tissue of aging primates. Mechanisms of Ageing and Development 2007;128:36-44.

(58) Ressler S, Bartkova J, Niederegger H, Bartek J, Scharffetter-Kochanek K, Jansen-Durr P, Wlaschek M. p16INK4A is a robust in vivo biomarker of cellular aging in human skin. Aging Cell 2006;5:379-389.

(59) Chang N, Yi J, Guo G, Liu X, Shang Y, Tong T, Cui Q, Zhan M, Gorospe M, Wang W. HuR uses AUF1 as a cofactor to promote p16INK4 mRNA decay. Mol Cell Biol 2010;30:3875-3886.

(60) Wang W, Martindale JL, Yang X, Chrest FJ, Gorospe M. Increased stability of the p16 mRNA with replicative senescence. EMBO Rep 2005;6:158-164.

(61) Welcker M, Lukas J, Strauss M, Bartek J. Enhanced protein stability: a novel mechanism of D-type cyclin over-abundance identified in human sarcoma cells. Oncogene 1996;13:419-425.

(62) Al-Khalaf HH, Hendrayani SF, Aboussekhra A. The Atr Protein Kinase Controls UV-Dependent Upregulation of p16INK4A Through Inhibition of Skp2-Related Polyubiquitination/Degradation. Mol Cancer Res 2011;9:311-319.

(63) Collins CJ, Sedivy JM. Involvement of the INK4a/Arf gene locus in senescence. Aging Cell 2003;2:145-150.

(64) Herbig U, Ferreira M, Condel L, Carey D, Sedivy JM. Cellular senescence in aging primates. Science 2006;311:1257.

(65) Yanagisawa K, Kosaka A, Iwahana H, Nakanishi M, Tominaga S. Opposite regulation of the expression of cyclin-dependent kinase inhibitors during contact inhibition. J Biochem 1999;125:36-40.

Supplemental Table 1. List of 215 probes which were differentially expressed between fibroblast strains from young and old subjects

ID_REF	Log fold change	Fold change	Average Expression	t	*P* value	Adjusted *P* value	Beta	Systematic Name	Gene Symbol	GeneName
34090	-0.38	-1.46	7.48	-13.71	1.44E-14	6.49E-10	22.33	NM_058197	CDKN2A	cyclin-dependent kinase inhibitor 2A (melanoma, p16, inhibits CDK4)
1631	-0.21	-1.24	5.79	-11.82	6.64E-13	2.99E-08	18.93	NM_000132	F8	coagulation factor VIII, procoagulant component (hemophilia A)
9872	-1.08	-2.94	7.21	-11.53	1.23E-12	5.52E-08	18.38	NM_000063	C2	complement component 2
14382	0.20	1.22	5.84	11.39	1.67E-12	7.50E-08	18.10	NM_053042	KIAA1729	KIAA1729 protein
27247	-0.38	-1.46	7.58	-11.09	3.24E-12	1.46E-07	17.50	NM_058197	CDKN2A	cyclin-dependent kinase inhibitor 2A (melanoma, p16, inhibits CDK4)
16994	-0.30	-1.35	8.27	-10.87	5.29E-12	2.38E-07	17.05	NM_025163	PIGZ	phosphatidylinositol glycan anchor biosynthesis, class Z
44819	-0.36	-1.44	7.33	-10.71	7.49E-12	3.37E-07	16.73	NM_058197	CDKN2A	cyclin-dependent kinase inhibitor 2A (melanoma, p16, inhibits CDK4)
16344	-0.37	-1.45	7.58	-10.62	9.23E-12	4.16E-07	16.54	NM_058197	CDKN2A	cyclin-dependent kinase inhibitor 2A (melanoma, p16, inhibits CDK4)
13213	-0.38	-1.46	7.55	-10.56	1.05E-11	4.73E-07	16.42	NM_058197	CDKN2A	cyclin-dependent kinase inhibitor 2A (melanoma, p16, inhibits CDK4)
23491	-0.61	-1.84	6.30	-10.18	2.57E-11	1.16E-06	15.60	NM_001034850	FLJ20152	hypothetical protein FLJ20152
33922	-0.42	-1.52	5.95	-9.76	6.82E-11	3.07E-06	14.70	NM_000063	C2	complement component 2
38638	-0.34	-1.40	8.59	-9.58	1.06E-10	4.77E-06	14.29	NM_001116	ADCY9	adenylate cyclase 9
7444	0.21	1.23	8.03	9.31	2.04E-10	9.16E-06	13.68	NM_004704	RRP9	RRP9, small subunit (SSU) processome component, homolog (yeast)
32445	-0.32	-1.38	7.61	-9.15	3.04E-10	1.37E-05	13.31	NM_058197	CDKN2A	cyclin-dependent kinase inhibitor 2A (melanoma, p16, inhibits CDK4)
8451	0.41	1.50	5.90	9.10	3.46E-10	1.56E-05	13.18	NM_006546	IGF2BP1	insulin-like growth factor 2 mRNA binding protein 1
20244	-0.41	-1.51	6.11	-9.05	3.88E-10	1.75E-05	13.08	NM_138554	TLR4	toll-like receptor 4
41115	-0.21	-1.23	5.77	-8.99	4.51E-10	2.03E-05	12.94	NM_153487	MDGA1	MAM domain containing glycosylphosphatidylinositol anchor 1
13770	0.36	1.43	5.56	8.76	7.94E-10	3.57E-05	12.41	NM_005503	APBA2	amyloid beta (A4) precursor protein-binding, family A, member 2 (X11-like)
21416	0.48	1.62	5.81	8.61	1.18E-09	5.32E-05	12.03	NM_198159	MITF	microphthalmia-associated transcription factor
36293	-0.51	-1.66	8.85	-8.54	1.38E-09	6.22E-05	11.89	NM_032823	C9orf3	chromosome 9 open reading frame 3
32467	-0.73	-2.07	6.33	-8.43	1.86E-09	8.38E-05	11.61	NM_053276	VIT	vitrin
36113	-0.74	-2.09	8.71	-8.42	1.91E-09	8.58E-05	11.58	AF010236		
23396	-0.33	-1.40	7.66	-8.41	1.93E-09	8.67E-05	11.57	NM_058197	CDKN2A	cyclin-dependent kinase inhibitor 2A (melanoma, p16, inhibits CDK4)
11285	-0.25	-1.29	5.58	-8.39	2.06E-09	9.29E-05	11.51	NM_001034850	FLJ20152	hypothetical protein FLJ20152
8703	0.14	1.15	6.31	8.33	2.42E-09	1.09E-04	11.36	NM_177559	CSNK2A1	casein kinase 2, alpha 1 polypeptide
17352	-0.88	-2.41	5.83	-8.31	2.49E-09	1.12E-04	11.33	BC041856	LOC400879	hypothetical gene supported by AK096951
8334	-0.34	-1.40	5.86	-8.29	2.62E-09	1.18E-04	11.28	NM_138554	TLR4	toll-like receptor 4
42807	-0.24	-1.28	6.28	-8.24	3.02E-09	1.36E-04	11.15	NM_052937	PCMTD1	protein-L-isoaspartate (D-aspartate) O-methyltransferase domain containing 1
29312	-0.48	-1.62	7.14	-8.23	3.09E-09	1.39E-04	11.13	A_32_P225328		
29118	-0.32	-1.37	7.54	-8.23	3.09E-09	1.39E-04	11.13	NM_058197	CDKN2A	cyclin-dependent kinase inhibitor 2A (melanoma, p16, inhibits CDK4)
2500	-0.30	-1.35	5.78	-8.22	3.16E-09	1.42E-04	11.11	NM_138554	TLR4	toll-like receptor 4
12396	0.63	1.87	6.37	8.21	3.29E-09	1.48E-04	11.07	BC018626		
36691	-0.33	-1.39	5.78	-8.06	4.84E-09	2.18E-04	10.70	NM_138554	TLR4	toll-like receptor 4
41441	-0.52	-1.68	6.04	-8.00	5.58E-09	2.51E-04	10.57	NM_017549	EPDR1	ependymin related protein 1 (zebrafish)
31781	-0.34	-1.40	5.88	-7.97	6.16E-09	2.77E-04	10.48	NM_138554	TLR4	toll-like receptor 4
22430	0.19	1.20	5.56	7.96	6.27E-09	2.82E-04	10.46	THC2657663		
41609	-0.31	-1.36	5.73	-7.95	6.36E-09	2.86E-04	10.45	NM_138554	TLR4	toll-like receptor 4
12121	0.30	1.35	5.87	7.90	7.28E-09	3.27E-04	10.32	NM_022897	RANBP17	RAN binding protein 17
38751	-0.17	-1.18	5.95	-7.76	1.05E-08	4.72E-04	9.97	NM_001099407	C20orf12	chromosome 20 open reading frame 12
15998	-0.35	-1.41	7.49	-7.76	1.06E-08	4.76E-04	9.97	BC012888	NDST1	N-deacetylase/N-sulfotransferase (heparan glucosaminyl) 1
44393	-0.23	-1.26	10.21	-7.76	1.07E-08	4.81E-04	9.96	NM_017983	WIPI1	WD repeat domain, phosphoinositide interacting 1
14866	-0.50	-1.66	7.35	-7.75	1.07E-08	4.83E-04	9.95	NM_000147	FUCA1	fucosidase, alpha-L- 1, tissue
9503	-0.32	-1.37	5.84	-7.67	1.34E-08	6.03E-04	9.74	NM_138554	TLR4	toll-like receptor 4
44741	-0.15	-1.16	6.55	-7.63	1.49E-08	6.70E-04	9.64	NM_198181	FLJ40113	golgi autoantigen, golgin subfamily a-like pseudogene
39212	1.05	2.86	7.39	7.62	1.55E-08	6.97E-04	9.60	NM_006547	IGF2BP3	insulin-like growth factor 2 mRNA binding protein 3
32971	0.84	2.31	6.65	7.57	1.76E-08	7.90E-04	9.48	NM_021076	NEFH	neurofilament, heavy polypeptide 200kDa
10808	0.15	1.16	9.91	7.54	1.89E-08	8.51E-04	9.41	NM_006559	KHDRBS1	KH domain containing, RNA binding, signal transduction associated 1
31481	-0.29	-1.34	5.82	-7.54	1.92E-08	8.63E-04	9.40	NM_138554	TLR4	toll-like receptor 4
21362	-0.62	-1.86	7.54	-7.52	1.98E-08	8.91E-04	9.37	NM_025225	PNPLA3	patatin-like phospholipase domain containing 3
9389	1.43	4.19	8.44	7.52	2.01E-08	9.06E-04	9.35	XR_018843	LOC649233	similar to Keratin, type I cytoskeletal 18 (Cytokeratin-18) (CK-18) (Keratin-18) (K18)
38867	1.28	3.59	7.16	7.46	2.37E-08	1.06E-03	9.20	XR_019231	LOC442249	hypothetical LOC442249
40424	0.57	1.77	5.95	7.44	2.47E-08	1.11E-03	9.16	NM_198159	MITF	microphthalmia-associated transcription factor
22402	-0.34	-1.41	5.91	-7.42	2.64E-08	1.19E-03	9.10	NM_138554	TLR4	toll-like receptor 4
10241	0.22	1.24	11.21	7.39	2.84E-08	1.28E-03	9.03	NM_000610	CD44	CD44 molecule (Indian blood group)
36253	0.18	1.20	7.84	7.38	2.90E-08	1.31E-03	9.01	NM_044472	CDC42	cell division cycle 42 (GTP binding protein, 25kDa)
11681	0.14	1.15	6.33	7.36	3.06E-08	1.38E-03	8.96	NM_177559	CSNK2A1	casein kinase 2, alpha 1 polypeptide
11737	-0.52	-1.69	6.93	-7.35	3.17E-08	1.42E-03	8.92	NM_002073	GNAZ	guanine nucleotide binding protein (G protein), alpha z polypeptide
1686	0.30	1.35	6.00	7.34	3.27E-08	1.47E-03	8.90	NM_182520	C22orf15	chromosome 22 open reading frame 15
28832	-0.38	-1.46	6.19	-7.31	3.47E-08	1.56E-03	8.84	NM_020777	SORCS2	sortilin-related VPS10 domain containing receptor 2
2909	-0.31	-1.36	5.59	-7.29	3.69E-08	1.66E-03	8.78	NM_000063	C2	complement component 2
44689	1.20	3.32	6.96	7.27	3.94E-08	1.77E-03	8.72	A_24_P383660	LOC643471	similar to Keratin, type I cytoskeletal 18 (Cytokeratin-18) (CK-18) (Keratin-18) (K18)
42458	-0.40	-1.50	8.91	-7.26	3.99E-08	1.79E-03	8.71	NM_012156	EPB41L1	erythrocyte membrane protein band 4,1-like 1
36702	-0.27	-1.31	7.95	-7.26	4.01E-08	1.80E-03	8.70	NM_001002009	NT5C3	5'-nucleotidase, cytosolic III
34895	1.19	3.29	7.03	7.21	4.64E-08	2.09E-03	8.56	A_24_P418687	LOC731794	similar to Keratin, type I cytoskeletal 18 (Cytokeratin-18) (CK-18) (Keratin-18) (K18)
12527	1.43	4.17	8.55	7.20	4.69E-08	2.11E-03	8.55	NM_000224	KRT18	keratin 18
33355	1.31	3.72	7.68	7.20	4.69E-08	2.11E-03	8.55	A_24_P161733		
6848	1.34	3.81	7.42	7.20	4.75E-08	2.13E-03	8.54	NM_000224	KRT18	keratin 18
9893	0.26	1.29	10.20	7.20	4.77E-08	2.14E-03	8.54	NM_001152	SLC25A5	solute carrier family 25 (mitochondrial carrier; adenine nucleotide translocator), member 5
10253	-0.76	-2.14	5.74	-7.19	4.87E-08	2.19E-03	8.52	BG118529		
16140	-0.17	-1.19	6.42	-7.18	4.96E-08	2.23E-03	8.50	NM_052937	PCMTD1	protein-L-isoaspartate (D-aspartate) O-methyltransferase domain containing 1
38804	1.79	6.00	7.06	7.15	5.43E-08	2.44E-03	8.41	NM_018476	BEX1	brain expressed, X-linked 1
17731	-0.60	-1.83	7.43	-7.12	5.87E-08	2.64E-03	8.34	NM_138554	TLR4	toll-like receptor 4

6264	0.26	1.30	8.83	7.12	5.88E-08	2.64E-03	8.34	NM_198216	SNRPB	small nuclear ribonucleoprotein polypeptides B and B1
12633	-0.08	-1.08	5.41	-7.12	5.96E-08	2.68E-03	8.32	NM_000132	F8	coagulation factor VIII, procoagulant component (hemophilia A)
23023	0.23	1.25	8.08	7.09	6.44E-08	2.89E-03	8.25	NM_178001	PPP2R4	protein phosphatase 2A, regulatory subunit B' (PR 53)
19790	-0.39	-1.48	8.51	-7.08	6.59E-08	2.96E-03	8.23	NM_032823	C9orf3	chromosome 9 open reading frame 3
1258	0.13	1.14	5.71	7.08	6.65E-08	2.99E-03	8.22	NM_014598	SOCS7	suppressor of cytokine signaling 7
14815	-0.19	-1.21	10.06	-7.07	6.78E-08	3.05E-03	8.20	NM_198868	TBC1D9B	TBC1 domain family, member 9B (with GRAM domain)
14598	0.15	1.16	9.18	7.06	6.87E-08	3.09E-03	8.19	NM_012247	SEPHS1	selenophosphate synthetase 1
25318	0.26	1.29	12.20	7.05	7.10E-08	3.19E-03	8.16	NM_001037808	EIF3S8	eukaryotic translation initiation factor 3, subunit 8, 110kDa
37363	-0.32	-1.37	6.37	-7.04	7.24E-08	3.25E-03	8.14	NM_031289	GSG1	germ cell associated 1
20510	0.48	1.62	8.14	7.04	7.29E-08	3.28E-03	8.13	NM_001970	EIF5A	eukaryotic translation initiation factor 5A
37652	-0.21	-1.23	11.25	-7.03	7.46E-08	3.35E-03	8.11	NM_152264	SLC39A13	solute carrier family 39 (zinc transporter), member 13
44533	-0.14	-1.15	5.34	-7.03	7.58E-08	3.40E-03	8.10	AK056135		
21753	-0.27	-1.31	6.26	-7.02	7.82E-08	3.51E-03	8.07	ENST00000270457	ZNF160	zinc finger protein 160
29622	-0.30	-1.35	6.29	-7.01	7.85E-08	3.53E-03	8.06	NM_000824	GLRB	glycine receptor, beta
4527	-0.32	-1.38	7.33	-6.96	9.01E-08	4.05E-03	7.93	NM_153208	IQCK	IQ motif containing K
7859	0.45	1.57	11.13	6.96	9.17E-08	4.12E-03	7.91	NM_199168	CXCL12	chemokine (C-X-C motif) ligand 12 (stromal cell-derived factor 1)
33380	-0.40	-1.49	8.41	-6.95	9.45E-08	4.25E-03	7.88	NM_000153	GALC	galactosylceramidase
38585	0.18	1.20	9.28	6.94	9.54E-08	4.29E-03	7.88	NM_016491	MRPL37	mitochondrial ribosomal protein L37
20182	1.83	6.24	7.58	6.94	9.57E-08	4.30E-03	7.87	NM_032621	BEX2	brain expressed X-linked 2
39594	-0.23	-1.26	9.69	-6.92	1.01E-07	4.55E-03	7.82	NM_016079	VPS24	vacuolar protein sorting 24 homolog (S, cerevisiae)
2154	-0.23	-1.26	7.04	-6.91	1.04E-07	4.68E-03	7.79	NM_005036	PPARA	peroxisome proliferator-activated receptor alpha
2770	1.04	2.84	6.48	6.89	1.11E-07	5.01E-03	7.73	XR_016695	LOC345430	similar to Keratin, type I cytoskeletal 18 (Cytokeratin-18) (CK-18) (Keratin-18) (K18)
32638	-0.35	-1.42	9.39	-6.88	1.13E-07	5.09E-03	7.71	NM_006291	TNFAIP2	tumor necrosis factor, alpha-induced protein 2
17317	-1.16	-3.19	8.59	-6.87	1.18E-07	5.28E-03	7.68	NM_017549	EPDR1	ependymin related protein 1 (zebrafish)
304	-0.11	-1.12	5.62	-6.86	1.20E-07	5.37E-03	7.66	AK091348		
4565	0.20	1.22	8.25	6.82	1.33E-07	5.97E-03	7.56	NM_007002	ADRM1	adhesion regulating molecule 1
7041	-0.15	-1.16	6.16	-6.82	1.33E-07	5.97E-03	7.56	NM_152331	ACOT4	acyl-CoA thioesterase 4
31016	-0.31	-1.37	5.90	-6.81	1.36E-07	6.10E-03	7.54	NM_138554	TLR4	toll-like receptor 4
6486	0.17	1.18	10.75	6.80	1.43E-07	6.43E-03	7.49	NM_001011724	RP11-78J21,1	heterogeneous nuclear ribonucleoprotein A1-like
19297	-0.35	-1.42	9.20	-6.78	1.47E-07	6.62E-03	7.46	NM_030786	SYNC1	syncoilin, intermediate filament 1
14513	0.15	1.16	9.61	6.78	1.49E-07	6.69E-03	7.45	NM_021243	C6orf115	chromosome 6 open reading frame 115
42541	-0.13	-1.14	6.32	-6.77	1.55E-07	6.94E-03	7.42	NM_002869	RAB6A	RAB6A, member RAS oncogene family
12338	1.23	3.42	7.21	6.76	1.58E-07	7.08E-03	7.40	XR_019330	LOC647162	similar to Keratin, type I cytoskeletal 18 (Cytokeratin-18) (CK-18) (Keratin-18) (K18)
27679	1.14	3.13	6.93	6.76	1.59E-07	7.14E-03	7.39	XR_019568	LOC343326	similar to Keratin, type I cytoskeletal 18 (Cytokeratin-18) (CK-18) (Keratin-18) (K18)
5415	0.15	1.16	6.22	6.75	1.64E-07	7.37E-03	7.36	NM_033637	BTRC	beta-transducin repeat containing
26043	-0.30	-1.35	6.06	-6.74	1.68E-07	7.57E-03	7.33	AA428090		
18066	-0.37	-1.44	8.09	-6.73	1.73E-07	7.75E-03	7.31	AK057167		
14884	1.16	3.18	6.81	6.72	1.75E-07	7.84E-03	7.30	XR_016590	LOC647913	similar to keratin complex 1, acidic, gene 18
22348	1.28	3.58	7.69	6.72	1.77E-07	7.97E-03	7.28	XR_018193	LOC391819	similar to Keratin, type I cytoskeletal 18 (Cytokeratin-18) (CK-18) (Keratin-18) (K18)
41523	-0.24	-1.27	7.30	-6.71	1.79E-07	8.05E-03	7.28	NM_003144	SSR1	signal sequence receptor, alpha (translocon-associated protein alpha)
3098	0.25	1.28	6.94	6.71	1.79E-07	8.06E-03	7.27	XM_001718519		
6769	0.25	1.28	9.03	6.71	1.84E-07	8.25E-03	7.25	NM_012322	LSM5	LSM5 homolog, U6 small nuclear RNA associated (S, cerevisiae)
13046	-0.24	-1.28	7.67	-6.70	1.89E-07	8.48E-03	7.23	AK095603	KIAA1822	KIAA1822
5070	0.23	1.26	10.54	6.69	1.91E-07	8.58E-03	7.21	NM_003146	SSRP1	structure specific recognition protein 1
19228	-0.44	-1.55	6.86	-6.68	1.95E-07	8.76E-03	7.19	AF131762		
29456	-0.28	-1.33	7.38	-6.68	1.96E-07	8.81E-03	7.19	AV721971		
18366	-0.07	-1.08	5.38	-6.67	2.01E-07	9.02E-03	7.17	NM_018902	PCDHA11	protocadherin alpha 11
2943	0.16	1.18	6.25	6.67	2.04E-07	9.17E-03	7.15	NM_177559	CSNK2A1	casein kinase 2, alpha 1 polypeptide
6232	0.15	1.16	8.03	6.67	2.05E-07	9.19E-03	7.15	NM_003863	DPM2	dolichyl-phosphate mannosyltransferase polypeptide 2, regulatory subunit
20957	0.35	1.42	8.90	6.66	2.09E-07	9.36E-03	7.13	NM_033274	ADAM19	ADAM metallopeptidase domain 19 (meltrin beta)
12807	1.24	3.44	7.41	6.65	2.13E-07	9.57E-03	7.11	XR_018311	LOC139060	similar to Keratin, type I cytoskeletal 18 (Cytokeratin-18) (CK-18) (Keratin-18) (K18)
38821	-0.33	-1.39	9.04	-6.65	2.14E-07	9.59E-03	7.11	NM_024692	RSNL2	restin-like 2
21311	0.42	1.52	8.67	6.65	2.14E-07	9.62E-03	7.11	NM_001970	EIF5A	eukaryotic translation initiation factor 5A
649	1.08	2.94	6.61	6.65	2.15E-07	9.64E-03	7.10	XR_018938	LOC132391	similar to Keratin, type I cytoskeletal 18 (Cytokeratin-18) (CK-18) (Keratin-18) (K18)
34773	-0.31	-1.37	6.35	-6.63	2.25E-07	1.01E-02	7.06	NM_078487	CDKN2B	cyclin-dependent kinase inhibitor 2B (p15, inhibits CDK4)
19295	0.47	1.60	5.92	6.61	2.37E-07	1.06E-02	7.01	THC2535223		
35951	-0.93	-2.55	8.21	-6.61	2.39E-07	1.07E-02	7.00	NM_005532	IFI27	interferon, alpha-inducible protein 27
10887	1.19	3.27	6.95	6.61	2.42E-07	1.08E-02	6.99	XR_017211	LOC651696	similar to Keratin, type I cytoskeletal 18 (Cytokeratin-18) (CK-18) (Keratin-18) (K18)
33899	-0.30	-1.34	7.12	-6.60	2.45E-07	1.10E-02	6.98	NM_002971	SATB1	special AT-rich sequence binding protein 1 (binds to nuclear matrix/scaffold-associating DNA's)
4209	0.14	1.15	5.52	6.59	2.51E-07	1.13E-02	6.95	XR_018641	LOC649545	similar to Keratin, type II cytoskeletal 8 (Cytokeratin-8) (CK-8) (Keraton-8) (K8)
38629	1.06	2.88	6.62	6.59	2.52E-07	1.13E-02	6.95	XR_019037	LOC391271	hypothetical LOC391271
40982	0.89	2.43	6.21	6.58	2.61E-07	1.17E-02	6.92	A_24_P6850		
36957	-0.19	-1.21	8.06	-6.58	2.61E-07	1.17E-02	6.92	NM_014781	RB1CC1	RB1-inducible coiled-coil 1
14987	-0.20	-1.23	8.01	-6.57	2.66E-07	1.20E-02	6.90	NM_012319	SLC39A6	solute carrier family 39 (zinc transporter), member 6
40074	-0.15	-1.16	7.16	-6.56	2.71E-07	1.22E-02	6.88	NM_016302	CRBN	cereblon
30487	1.06	2.88	6.70	6.56	2.71E-07	1.22E-02	6.88	XR_018749	LOC442405	similar to Keratin, type I cytoskeletal 18 (Cytokeratin-18) (CK-18) (Keratin-18) (K18)
40222	0.31	1.36	6.92	6.56	2.73E-07	1.22E-02	6.88	NM_021214	LOC58489	hypothetical protein from EUROIMAGE 588495
18800	-0.24	-1.28	8.44	-6.56	2.74E-07	1.23E-02	6.87	NM_021626	SCPEP1	serine carboxypeptidase 1
34991	-0.73	-2.08	6.89	-6.55	2.84E-07	1.27E-02	6.84	NM_014737	RASSF2	Ras association (RalGDS/AF-6) domain family 2
31712	-0.12	-1.12	5.49	-6.54	2.90E-07	1.30E-02	6.82	NM_080676	C20orf133	chromosome 20 open reading frame 133
41927	-0.38	-1.46	11.98	-6.52	3.07E-07	1.38E-02	6.76	NM_212482	FN1	fibronectin 1
39571	-0.22	-1.25	5.96	-6.51	3.11E-07	1.40E-02	6.75	ENST00000328711		
10395	0.41	1.50	11.20	6.51	3.19E-07	1.43E-02	6.73	NM_199168	CXCL12	chemokine (C-X-C motif) ligand 12 (stromal cell-derived factor 1)
34939	-0.13	-1.13	6.57	-6.49	3.35E-07	1.50E-02	6.68	THC2505349		
3557	-0.32	-1.37	7.03	-6.48	3.42E-07	1.53E-02	6.66	NM_032549	IMMP2L	IMP2 inner mitochondrial membrane peptidase-like (S, cerevisiae)
16302	-0.16	-1.17	7.04	-6.48	3.44E-07	1.54E-02	6.65	XR_019214	LOC649551	similar to nuclear receptor binding factor 2
4882	0.23	1.26	10.04	6.48	3.45E-07	1.55E-02	6.65	THC2509446		
11654	0.17	1.18	11.39	6.46	3.61E-07	1.62E-02	6.61	NM_000610	CD44	CD44 molecule (Indian blood group)
9170	-0.89	-2.45	8.34	-6.46	3.66E-07	1.64E-02	6.60	NM_005532	IFI27	interferon, alpha-inducible protein 27
37711	-0.26	-1.30	7.24	-6.44	3.88E-07	1.74E-02	6.54	NM_001038628	B3GALNT1	beta-1,3-N-acetylgalactosaminyltransferase 1 (globoside blood group)
32308	1.25	3.47	7.36	6.43	3.89E-07	1.74E-02	6.54	NM_173624	FLJ40504	hypothetical protein FLJ40504

4695	-0.35	-1.42	12.09	-6.41	4.22E-07	1.89E-02	6.46	NM_212482	FN1	fibronectin 1
12773	0.09	1.09	9.82	6.39	4.36E-07	1.95E-02	6.43	NM_013235	RNASEN	ribonuclease III, nuclear
1999	1.15	3.15	6.80	6.39	4.38E-07	1.96E-02	6.42	XR_019198	LOC391589	similar to Keratin, type I cytoskeletal 18 (Cytokeratin-18) (CK-18) (Keratin-18) (K18)
3756	-0.93	-2.53	8.18	-6.38	4.51E-07	2.02E-02	6.39	NM_005532	IFI27	interferon, alpha-inducible protein 27
23972	-0.34	-1.41	11.58	-6.38	4.57E-07	2.05E-02	6.38	NM_015170	SULF1	sulfatase 1
40185	-0.19	-1.21	10.94	-6.37	4.70E-07	2.11E-02	6.35	NM_001018108	SERF2	small EDRK-rich factor 2
39793	0.16	1.18	8.03	6.36	4.73E-07	2.12E-02	6.35	NM_012267	HSPBP1	hsp70-interacting protein
11020	1.23	3.42	7.43	6.36	4.79E-07	2.15E-02	6.34	THC2524582		
24675	-0.29	-1.34	12.21	-6.36	4.79E-07	2.15E-02	6.34	NM_212482	FN1	fibronectin 1
13271	-0.12	-1.13	10.59	-6.35	4.97E-07	2.23E-02	6.30	NM_004872	TMEM59	transmembrane protein 59
9064	-0.24	-1.28	7.10	-6.34	5.02E-07	2.25E-02	6.29	NM_014039	C11orf54	chromosome 11 open reading frame 54
35349	-0.12	-1.13	5.85	-6.34	5.03E-07	2.26E-02	6.29	AK024516		
11062	0.20	1.23	8.46	6.33	5.23E-07	2.34E-02	6.25	NM_006555	YKT6	YKT6 v-SNARE homolog (S, cerevisiae)
44582	-0.18	-1.19	8.03	-6.33	5.24E-07	2.35E-02	6.25	NM_033407	DOCK7	dedicator of cytokinesis 7
28684	-0.15	-1.16	8.01	-6.32	5.31E-07	2.38E-02	6.24	NM_016446	C9orf127	chromosome 9 open reading frame 127
41988	0.16	1.18	7.73	6.30	5.73E-07	2.57E-02	6.17	NM_044472	CDC42	cell division cycle 42 (GTP binding protein, 25kDa)
14270	-0.33	-1.39	10.75	-6.28	6.00E-07	2.69E-02	6.12	NM_000366	TPM1	tropomyosin 1 (alpha)
8943	-0.26	-1.30	7.56	-6.28	6.03E-07	2.70E-02	6.12	NM_058197	CDKN2A	cyclin-dependent kinase inhibitor 2A (melanoma, p16, inhibits CDK4)
13215	1.03	2.80	6.49	6.28	6.06E-07	2.72E-02	6.11	XR_018953	LOC391179	similar to Keratin, type I cytoskeletal 18 (Cytokeratin-18) (CK-18) (Keratin-18) (K18)
27651	0.38	1.47	6.96	6.27	6.15E-07	2.76E-02	6.10	NM_002655	PLAG1	pleiomorphic adenoma gene 1
5168	-0.19	-1.21	8.13	-6.27	6.15E-07	2.76E-02	6.10	NM_178564	NRBP2	nuclear receptor binding protein 2
27609	0.11	1.12	6.38	6.27	6.23E-07	2.79E-02	6.09	NM_177559	CSNK2A1	casein kinase 2, alpha 1 polypeptide
43036	1.04	2.82	6.73	6.25	6.55E-07	2.94E-02	6.04	XR_018420	LOC391827	similar to Keratin, type I cytoskeletal 18 (Cytokeratin-18) (CK-18) (Keratin-18) (K18)
40951	0.24	1.27	6.77	6.24	6.63E-07	2.97E-02	6.03	NM_007212	RNF2	ring finger protein 2
959	1.13	3.09	6.90	6.24	6.65E-07	2.98E-02	6.02	A_24_P281443	LOC649375	similar to Keratin, type I cytoskeletal 18 (Cytokeratin-18) (CK-18) (Keratin-18) (K18)
1296	1.31	3.72	7.65	6.24	6.71E-07	3.01E-02	6.02	XR_019191	LOC121054	similar to Keratin, type I cytoskeletal 18 (Cytokeratin-18) (CK-18) (Keratin-18) (K18)
9569	0.98	2.67	6.41	6.24	6.76E-07	3.03E-02	6.01	XR_019060	LOC644030	similar to Keratin, type I cytoskeletal 18 (Cytokeratin-18) (CK-18) (Keratin-18) (K18)
6183	-0.34	-1.40	12.08	-6.23	6.87E-07	3.08E-02	5.99	NM_212482	FN1	fibronectin 1
7752	-0.54	-1.72	9.02	-6.23	6.87E-07	3.08E-02	5.99	NM_003392	WNT5A	wingless-type MMTV integration site family, member 5A
16674	-0.32	-1.37	12.16	-6.22	7.02E-07	3.15E-02	5.97	NM_212482	FN1	fibronectin 1
752	0.18	1.20	8.48	6.22	7.16E-07	3.21E-02	5.95	NM_017722	TRMT1	TRM1 tRNA methyltransferase 1 homolog (S, cerevisiae)
36709	-0.34	-1.41	8.55	-6.22	7.17E-07	3.21E-02	5.95	NM_183233	SLC22A18	solute carrier family 22 (organic cation transporter), member 18
25357	-1.18	-3.27	7.94	-6.22	7.17E-07	3.21E-02	5.95	NM_000954	PTGDS	prostaglandin D2 synthase 21kDa (brain)
15294	-0.24	-1.27	9.98	-6.20	7.52E-07	3.37E-02	5.91	NM_017823	DUSP23	dual specificity phosphatase 23
34641	0.16	1.17	7.90	6.19	7.66E-07	3.43E-02	5.89	NM_044472	CDC42	cell division cycle 42 (GTP binding protein, 25kDa)
19368	0.12	1.13	6.94	6.18	7.87E-07	3.53E-02	5.86	NM_005702	ERAL1	Era G-protein-like 1 (E, coli)
2342	-0.13	-1.14	5.43	-6.18	7.96E-07	3.57E-02	5.85	NM_002302	LECT2	leukocyte cell-derived chemotaxin 2
27606	0.14	1.15	9.48	6.17	8.07E-07	3.62E-02	5.84	NM_006392	NOL5A	nucleolar protein 5A (56kDa with KKE/D repeat)
3553	0.22	1.24	8.66	6.17	8.14E-07	3.65E-02	5.83	NM_018188	ATAD3A	ATPase family, AAA domain containing 3A
2158	0.05	1.05	5.32	6.16	8.44E-07	3.78E-02	5.80	XR_018787	LOC339396	similar to neurofilament, heavy polypeptide
7946	0.18	1.19	8.61	6.16	8.46E-07	3.79E-02	5.79	NM_007002	ADRM1	adhesion regulating molecule 1
2841	0.16	1.17	10.61	6.16	8.50E-07	3.81E-02	5.79	A_32_P179205	LOC402562	similar to Heterogeneous nuclear ribonucleoprotein A1 (Helix-destabilizing protein) (Single-strand binding protein) (hnRNP core protein A1) (HDP-1) (Topoisomerase-inhibitor suppressed)
41866	-0.15	-1.17	6.46	-6.15	8.60E-07	3.85E-02	5.78	NM_007202	AKAP10	A kinase (PRKA) anchor protein 10
30168	0.08	1.09	5.36	6.15	8.71E-07	3.91E-02	5.77	AK056119		
6538	-0.26	-1.30	9.98	-6.14	8.89E-07	3.99E-02	5.75	NM_001343	DAB2	disabled homolog 2, mitogen-responsive phosphoprotein (Drosophila)
41042	0.21	1.24	10.01	6.13	9.02E-07	4.04E-02	5.73	NM_004515	ILF2	interleukin enhancer binding factor 2, 45kDa
7984	0.36	1.43	9.18	6.12	9.30E-07	4.17E-02	5.70	NM_021214	LOC58489	hypothetical protein from EUROIMAGE 588495
44649	0.99	2.68	6.56	6.12	9.32E-07	4.18E-02	5.70	XR_018462	LOC391803	similar to Keratin, type I cytoskeletal 18 (Cytokeratin-18) (CK-18) (Keratin-18) (K18)
13274	-0.32	-1.37	6.72	-6.12	9.40E-07	4.21E-02	5.69	ENST00000393500		
31708	0.20	1.22	6.56	6.12	9.51E-07	4.26E-02	5.68	NM_024821	CCDC134	coiled-coil domain containing 134
33989	-0.18	-1.20	6.92	-6.11	9.68E-07	4.34E-02	5.67	NM_004348	RUNX2	runt-related transcription factor 2
33242	-0.19	-1.21	6.88	-6.10	9.84E-07	4.41E-02	5.65	NM_001122838	NAPE-PLD	N-acyl-phosphatidylethanolamine-hydrolyzing phospholipase D
5588	0.22	1.25	9.37	6.10	9.93E-07	4.45E-02	5.64	NM_000190	HMBS	hydroxymethylbilane synthase
38712	-0.24	-1.27	9.88	-6.09	1.01E-06	4.52E-02	5.63	NM_005780	LHFP	lipoma HMGIC fusion partner
11818	-0.27	-1.31	5.45	-6.09	1.03E-06	4.60E-02	5.61	NM_016953	PDE11A	phosphodiesterase 11A
25250	-0.84	-2.33	8.25	-6.08	1.04E-06	4.64E-02	5.60	NM_005532	IFI27	interferon, alpha-inducible protein 27
39603	-0.24	-1.27	6.09	-6.08	1.05E-06	4.72E-02	5.59	NM_001033045	GPR155	G protein-coupled receptor 155
39313	-0.16	-1.18	5.46	-6.08	1.06E-06	4.73E-02	5.58	NM_181643	C1orf88	chromosome 1 open reading frame 88
7675	0.17	1.19	5.67	6.07	1.07E-06	4.79E-02	5.57	NM_000679	ADRA1B	adrenergic, alpha-1B-, receptor
41277	-0.20	-1.22	7.08	-6.07	1.08E-06	4.86E-02	5.56	NM_015061	JMJD2C	jumonji domain containing 2C
36866	-0.27	-1.32	8.69	-6.06	1.10E-06	4.91E-02	5.55	NM_152558	IQCE	IQ motif containing E
26233	1.03	2.80	6.64	6.06	1.11E-06	4.98E-02	5.53	A_24_P358406		

Supplemental table 2. ROS levels, Senescence Associated-β-gal activity and p16 expression measured at the mRNA level in non-stressed and rotenone stressed human fibroblasts from young and old subjects from the Leiden 85-plus Study. Values are given as mean (SE).

	Young	Old	p
Micro-array experiments	n=6	n=6	
SA-β-gal (MdFI)			
Non-stressed	2078 (357)	2634 (360)	0.045
Rotenone-induced increase	+11433 (463)	2395 (472)	0.056
p16 (fold change)			
array	1	1.46	**<0.0001**
qPCR Non-stressed	1	1.43 (0.08)	**0.005**
qPCR Rotenone, 3h	1	1.37 (0.14)	**0.060**
qPCR Rotenone, 3d	1	1.42 (0.11)	**0.031**
Replication experiments	n=10	n=10	
SA-β-gal (MdFI)			
Non-stressed	3146 (368)	22740 (363)	0.23
Rotenone-induced increase	+1132 (260)	+1638 (255)	**0.052**
p16 (fold change)			
qPCR Non-stressed, 3d	1	0.74 (0.05)	**<0.001**
qPCR Rotenone, 3d	1	0.99 (0.07)	0.52

Supplemental Figure 1. Variation in expression between strains from different subjects presented as a heatmap